Thermal buckling solutions of generic metallic and laminated structures: Total and updated Lagrangian formulations via refined beam elements

Journal of Thermal Stresses

ISSN: (Print) (Online) Journal homepage: https://www.tandfonline.com/loi/uths20

Thermal buckling solutions of generic metallic and laminated structures: Total and updated Lagrangian formulations via refined beam elements

Yang Yan, Alfonso Pagani & Erasmo Carrera

To cite this article: Yang Yan, Alfonso Pagani & Erasmo Carrera (2022) Thermal buckling solutions of generic metallic and laminated structures: Total and updated Lagrangian formulations via refined beam elements, Journal of Thermal Stresses, 45:8, 669-694, DOI: 10.1080/01495739.2022.2090471

To link to this article: https://doi.org/10.1080/01495739.2022.2090471

Published online: 28 Jul 2022.

JOURNAL OF THERMAL STRESSES
2022, VOL. 45, NO. 8, 669–694
https://doi.org/10.1080/01495739.2022.2090471

Thermal buckling solutions of generic metallic and laminated structures: Total and updated Lagrangian formulations via refined beam elements

Yang Yan[a], Alfonso Pagani[b], and Erasmo Carrera[b,c]

[a]School of Aeronautic Science and Engineering, Beihang University, Beijing, China; [b]Mul[2], Department of Mechanical and Aerospace Engineering, Politecnico di Torino, Torino, Italy; [c]Department of Mechanical Engineering, College of Engineering, Prince Mohammad Bin Fahd University, Al Khobar, Kingdom of Saudi Arabia

ABSTRACT

The thermal buckling behavior of metallic and laminated beams/plates is investigated using a linearized stability analysis. By selecting different reference frames, two distinct types of 3 D stability equations can be generated using total and updated Lagrangian formulations (TLF and ULF). Various beam theory kinematics can be obtained within the framework of 1 D Carrera Unified Formulation (CUF) by employing an arbitrary expansion of the generalized variables. More precisely, an improved hierarchical Legendre expansion (IHLE) is used to formulate the Layer-Wise (LW) model in a robust manner. Additionally, using a finite element approximation in conjunction with CUF-IHLE, the obtained stability equations are discretized into a set of algebraic equations. The critical temperatures predicted by TLF- and ULF-based CUF-IHLE models are compared using numerical examples of beams and plates with varying boundary conditions, lamination schemes, and thickness-to-width ratios. Both models are validated for correctness using the commercial software ABAQUS. Besides, the effect of strain distribution during the pre-buckling stage is evaluated in the plate-like structure using one- and two-step analyses.

ARTICLE HISTORY
Received 24 October 2021
Accepted 8 June 2022

KEYWORDS
Carrera Unified Formulation; improved hierarchical Legendre expansion; thermal buckling; total Lagrangian formulation; updated Lagrangian formulation

1. Introduction

In the aeronautical and space industries, sub-portions of several complicated structural topologies can be viewed as approximate to beam- and plate-like structures. For instance, skin panels can be idealized as plate/shell structures, whereas longitudinal stringers and transverse frames as beams. These structures frequently undergo severe aerodynamic heating after the speed of the vehicle exceeds Mach 2.2. Thus, the thermoelastic buckling problem that arises should be of major concern to designers and researchers [1]. By definition, the solution to the thermal buckling problem is to determine the critical temperature beyond which beam/plate structures enter another equilibrium state dominated by a bending mode in response to an external perturbation force. As a result, this temperature is also referred to as the thermal bifurcation point. Numerous scientists have committed their attention to this subject throughout the years, utilizing 1 D/2D structural theories. For the sake of completeness, the following is a brief and not exhaustive survey of the kinematic descriptions used for 1 D/2D models.

CONTACT Yang Yan yanyang864914630@126.com School of Aeronautic Science and Engineering, Beihang University, Xueyuan Road 37, 100191 Beijing, China.

One of the most well-known theories is the Euler-Bernoulli beam theory (EBBT), which presupposes that the cross section of the beam remains flat and perpendicular to the neutral axis of the beam before and after deformation. The buckling load can be determined using EBBT by solving differential equations in an analytical form known as Euler's column formula or or in an approximate form using the Rayleigh-Ritz method [2]. Based on EBBT, Elishakoff and his collaborators developed closed-form solutions for buckling of colums in terms of non-uniform Young's modulus [3], a variety of boundary conditions [4], and the combined action of concentrated and distributed loads [5]. Li and Batra [6] investigated the buckling modes and transitions among them of uniformly heated Euler–Bernoulli beams rested on nonlinear elastic foundations analytically. Sankar and Tzeng [7] derived an exact solution to the plane thermoelasticity issue for functionally graded beams based on EBBT under the premise of exponentially varying elastic constants and temperature. The only snag is that EBBT overestimates the buckling stresses of short beams due to its omission of shear deformation effects. As an alternative, Timoshenko beam theory (TBT) incorporates shear deformation effects by allowing the cross-section of beams to rotate about the neutral axis. Mathew et al. [8] studied the thermal buckling behavior of antisymmetric cross-ply composite laminates with regard to TBT. Kar and Sujata [9] investigated static buckling load and dynamic instability region of a Timoshenko beam with a thermal gradient lying on a variable Pastenak foundation. Wang [10] devised a B-spline Rayleigh–Ritz approach based on TBT for the analysis of free vibration and buckling issues in thin and thick beams and plates, and the method was found to be locking-insensitive. Notably, EBBT correlates to Kirchhoff–Love theory in plate structures, whereas TBT corresponds to Mindlin–Reissner theory. Morimoto [11] demonstrated how to define a new position of the reference plane for an inhomogeneous rectangular plate and then derived its fundamental equation in terms of arbitrary thermal loads based on Kirchhoff–Love theory. They also discussed the effect of the aspect ratio, width-to-thickness ratio, and inhomogeneity parameter on the critical temperature. Prabhu and Dhanaraj [12] conducted thermoelasticity and thermal buckling analysis on symmetrically laminated composite plates using Mindlin–Reissner theory. Li et al. [13] presented analytical solutions to the buckling and vibro-acoustic problems of the clamped composite laminated plate in the thermal environment using Kirchhoff–Love and Mindlin–Reissner theories, respectively. Additionally, the aforesaid theory has made contributions to the thermal buckling of micro and nano beams and plates through the work of Mohammadabadi et al. [14], Ebrahimi and Salari [15], Taati [16], Wang et al. [17], and Shojaeefard et al. [18]. Although extensively employed, TBT requires the definition of a shear correction factor to ensure that the unloaded lateral surfaces have zero shear stress. As reported by Omidvar [19], and Madabhusi-Raman and Davalos [20], the definition of the shear correction factor depends on many factors, e.g., the structural geometry dimension, material property, lamination scheme, loading form, and boundary condition, etc.

Accordingly, numerous higher-order shear deformation theories (HSDT) have been presented in order to eliminate the need for the shear correction factor. Lezgy-Nazargah [21] used isogeometric analysis to conduct a thorough coupled thermal-mechanical analysis of bidirectional functionally graded beams. The in-plane displacement field introduced in his work is approximated via a combination of polynomial and exponential expressions, resulting in a refined high order global–local theory. Shafiei and She [22] employed HSDT to deal with the problem of thermally induced vibration in functionally graded nano-tubes. Such a kind of HSDT characterizes the through-the-thickness variation of the axial displacement field with polynomial functions. By incorporating a shape function into the approximation of the longitudinal displacement vector, Aydogdu [23] developed a unified three-degree-of-freedom beam theory. Thus, Reddy's parabolic shear deformation beam theory [24], Soldatos's hyperbolic shear deformation beam theory [25], and Karama's shear deformation beam theory [26] can all be derived as special cases of this theory. In terms of the thermal buckling of cross-ply laminated beams, they discovered that some

cross-ply laminated beams buckle upon cooling rather than heating while others do not buckle regardless of whether they are heated or cooled. Van Do and Lee [27] developed a refined quasi-3D theory for thermal buckling analysis of perfect and imperfect functionally graded plates by including transverse shear and transverse normal shape functions in the description of in-plane and out-of-plane displacements, respectively, confirming the importance of including thickness expansion effects in thermal buckling assessments of functionally graded plates. Cetkovic [28] used Layer-Wise (LW) description of in-plane displacement components and quadratic variation of transverse displacement to derive thermal buckling solutions for laminated composite plates, including Navier's analytical solution in the strong form and the finite element solution in the weak form. The full LW definition of a 3 D displacement field is used in the work of Shariyat [29], in which the instability temperature of composite multilayered plates with temperature-dependent properties can be calculated via a modified Budiansky criterion.

According to Koiter's suggestion [30], any refinement of classical theories may be deemed useless in the modeling of multilayered laminated structures until the effects of interlaminar continuous transverse shear and normal stresses are taken into account. In response to this consideration, Carrera [31] developed a uniform formulation, later dubbed the Carrera Unified Formulation (CUF). Within the framework of CUF, any structural theories can degenerate into a generalized kinematics that employs an arbitrary expansion of generalized variables, such as displacement or stress components. CUF was initially used to build 2 D models of plates and shells [32] and was then extended to beam (1 D) models [33]. Depending on the function used in the expansion, CUF can be further classified into the following categories: TE (Taylor expansion), LE (Lagrange expansion), CE (Chebyshev expansion), HLE (hierarchical Legendre expansion), and IHLE (improved hierarchical Legendre expansion). Nali et al. [34] developed the Equivalent Single Layer (ESL) model using 2 D CUF-TE to evaluate a large variety of 2 D models for buckling analysis of isotropic, orthotropic, and anisotropic plates under biaxial and shear stresses. They concluded that classical theories, such as Kirchhoff–Love and Mindlin–Reissner, are insufficient for modeling thick plates or multilayered plates made of laminae with a high orthotropic ratio. Fazzolari and Carrera [35] compared the critical temperature for a sandwich plate using 2 D CUF-TE and -HLE. They employed TE to implement ESL models and HLE to LW models. Vescovini [36] extended the work of [35] to predict the global and local buckling behaviors of sandwich plates with anisotropic facesheets and pointed out that the Ritz approach based on trigonometric functions produced significant inaccuracies in anisotropic plates with non-negligible bending/twisting coupling. Ibrahim et al. [37] applied 1 D CUF-TE to analyze the buckling of laminated beams and panels and emphasized the critical nature of higher-order terms in accurately predicting torsional modes. As an alternative to weak-form solutions, Carrera et al. [38] developed differential governing equations in strong form as an alternative to weak-form solutions using 1 D CUF-TE and tackled the buckling problem of thin-walled beams using the dynamic stiffness approach. Recently, Pagani and Sanchez-Majano [39,40] extended LW models (1 D CUF-LE and-HLE) to mesoscale and multiscale buckling assessments of variable angle tow laminates with the inclusion of uncertain defects, such as, fiber misalignment. The ESL model (1 D CUF-TE) was employed as a comparative model.

IHLE [41,42] is a more powerful, but elegant, model for CUF models with preexisting expansions. It is based on HLE models, inheriting all of its advantages, such as hierarchical kinematics and local refinement of the cross-section sub-domain, while deftly avoiding its disadvantage, i.e., the possibility of violating C_Z^0-Requirements [43], by transforming the hierarchical Legendre functions on the edge to Lagrange ones. Additionally, the remarkable advantages of HLE over TE and LE are reported in Pagani et al. [44]. By promoting expansion order in two orthogonal dimensions throughout the cross-section, 1 D CUF-IHLE can be considered an alternative to 2 D plate/shell models for the analysis of plates or cylindrical shells without requiring re-meshing operations, as 1 D CUF-LE does [39,40].

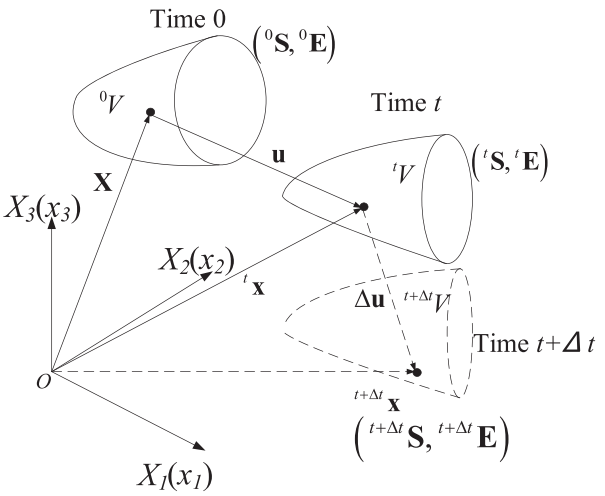

Figure 1. The geometrical configurations and the associated variables at different times.

Li and Song [45], and Zhou et al. [46] considered the buckling of thin panels exposed to a uniform temperature field as an in-plane stress problem, omitting the transverse normal stress. Additionally, they skipped pre-buckling analysis, assuming that when the boundary condition is simply supported, clamped, or a combination of the two, the pre-buckling stress state is dominated by uniform thermal stress. This form of buckling analysis will be referred to as one-step analysis hereafter. Obviously, due to the absence of pre-buckling analysis, rapid buckling analysis has a limited range of applicability, necessitating the need of integrated buckling analysis, referred to in this work as two-step analysis.

Carrera [47], on the other hand, emphasized the need of including the transverse normal strain effect in static thermoelastic analysis of thick homogeneous and multilayered plates. In this context, quasi-3D or three-dimensional thermal buckling assessment remains critical for high-fidelity solutions. CUF is capable of reproducing 3 D-like accuracy at a cheaper computing cost than 3 D solid elements by refining kinematics across the cross-section or thickness. Furthermore, classical buckling analysis can be converted to a standard eigenvalue problem by taking the increment of the nonlinear equilibrium equation, which is built using total Lagrangian description, i.e., the reference frame characterized by the undeformed configuration. As opposed to this, Vescovini et al. [48] used nonlinear eigenvalue prediction to determine the critical temperature of laminated and sandwich plates, taking into consideration nonlinear pre-buckling deformation in the thickness direction. They concluded that there is a discernible difference between the linear and nonlinear forecasts for thick plates or strong anisotropy in the lay-up, despite the fact that both predictions are capable of 3 D-like accuracy. However, the proposed approach confines the solution to immovable edge boundary conditions.

The purpose of this work is to demonstrate the feasibility of using 1 D CUF-IHLE for thermal buckling analysis of beams and plates using both total and updated Lagrangian formulations. The key novelties of the paper can be stated as follows: (i) the computational effort required by the present models is significantly less than that required by models based on 3 D FE discretizations; (ii) the systematic difference between the linearized total and updated Lagrangian formulations for thermal buckling analysis is unmasked; (iii) the use of the linearized updated Lagrangian formulation enables the quantification of the thermal buckling strength of structures of any thickness using a linear solver, avoiding the nonlinear eigenvalue analysis in the case of thick structures, as described in Vescovini et al. [48]; (iv) the proposed model is capable of resolving plate thermal buckling issues in both in-plane and three-dimensional descriptions. The remainder of this paper is structured as follows. To begin, Section 2 discusses thermal buckling in detail

using total and updated Lagrangian formulations; then, the CUF kinematic field and the IHLE formulation are explained in Section 3; Section 4 discusses the solution processes defined by one-step and two-step analyses, as well as the derivation of the fundamental nucleus within the context of total and updated Lagrangian formulations for pre-buckling and thermal buckling problems. In Section 5, the accuracy and efficiency of the proposed approach are validated by 3 D finite element analysis; comparisons between total and updated Lagrangian formulations, as well as one-step and two-step analyses are made by considering various thickness-to-length ratios, fiber orientation angles, and boundary conditions; and finally, some useful conclusions are drawn in Section 6.

2. Linearized variational equations in three-dimensional space

Figure 1 gives a deformable body whose configurations, indicated by ${}^0V, \ldots, {}^tV, {}^{t+\Delta t}V$, vary with the time ($t$). The position vectors of a particle are referred as $\mathbf{X}, \ldots, {}^t\mathbf{x}, {}^{t+\Delta t}\mathbf{x}$, where $\mathbf{X}$ is the material (or referential) coordinate, $\mathbf{x}$ the spatial (or current) coordinate, and the left superscript the current time. The crucial step in resolving the buckling problem is linearizing the variational equation, i.e., determining its increment at time t. Additionally, correct definitions of stress (${}^t\mathbf{S}$) and strain (${}^t\mathbf{E}$) tensors must be adopted in accordance with the reference frame. When different reference frames are chosen, however, separate models are constructed, namely the total Lagrangian formulation (TLF) and the updated Lagrangian formulation (ULF). Following that, we will take a quick look at the linearization process in terms of TLF and ULF. Further details on the derivation of the formula can be found in Kim [49] and Noguchi and Hisada [50].

2.1. Total Lagrangian formulation

Assume that the elastic continuum experiences a gradual change in temperature, resulting in a thermal-mechanical issue. Additionally, we define that the thermal and mechanical states that are generated are uncoupled. In other words, thermal and mechanical strains (${}^t\mathbf{E}^{th}$ and ${}^t\mathbf{E}$) can be independently analyzed. As specified above, the variational equation at time t is written in terms of material variables based on the initial (or undeformed) configuration; that is

$$\int_{{}_0V} \delta {}^t_0\mathbf{E} : {}^t_0\mathbf{S} \mathrm{d}^0V = \delta L_{\mathrm{ext}} \tag{1}$$

where the left subscript of a variable represents the chosen reference frame. δ is the variational operator; L_{ext} is the work done by the external load. Temperature cannot be viewed as the primary variable under the uncoupled hypothesis, i.e., $\delta {}^t\mathbf{E}^{th} = 0$. The second Piola-Kirchhoff stress tensor ${}^t_0\mathbf{S}$, the Green-Lagrange strain tensor ${}^t_0\mathbf{E}$, and the thermal strain ${}^t\mathbf{E}^{th}$ can be defined as

$$\begin{gathered}
{}^t_0\mathbf{E} = \frac{1}{2}\left((\nabla_0\mathbf{u})^{\mathrm{T}} + \nabla_0\mathbf{u} + \nabla_0\mathbf{u}\cdot(\nabla_0\mathbf{u})^{\mathrm{T}}\right), \quad {}^t_0E_{ij} = \frac{1}{2}\left(\frac{\partial u_i}{\partial X_j} + \frac{\partial u_j}{\partial X_i} + \frac{\partial u_k}{\partial X_i}\frac{\partial u_k}{\partial X_j}\right) \quad i,\ j = 1,2,3 \\
{}^t_0\mathbf{S} = \mathbf{C} : \left({}^t_0\mathbf{E} - {}^t\mathbf{E}^{th}\right), \quad {}^t_0S_{ij} = C_{ijkl}\ \left({}^t_0E_{kl} - {}^tE^{th}_{kl}\right) \quad i,\ j,\ k,\ l = 1,2,3 \\
{}^t\mathbf{E}^{th} = \Delta T\boldsymbol{\alpha}, \quad {}^tE^{th}_{ij} = \Delta T\alpha_{ij}, \quad \Delta T = {}^tT - {}^0T \quad i,\ j = 1,2,3
\end{gathered} \tag{2}$$

where the symbol ∇_0 specifies the material gradient; $\mathbf{u}$ is the displacement vector; the right subscript T stands for the transposition operator; $\mathbf{C}$ is the fourth-order constitutive tensor which is invariant with respect to the time variable t by assumption; ΔT signifies an increase in temperature over the reference temperature ${}^0T$; and $\boldsymbol{\alpha}$ denotes the thermal coefficient of expansion, which is believed to be a time-independent variable. Thermal strains are configuration independent as a result of this assumption.

Since $\Delta(\delta L_{\text{ext}})$ is zero in the case of the conservative loading, the linearization of the variational equation only acts on the left-hand side of Eq. (1), which can be simplified to the following form when the present and reference configurations are indistinguishable:

$$\Delta\left(\int_{0V}\delta_0^t\mathbf{E}:{}_0^t\mathbf{S}\mathrm{d}^0V\right)=\int_{0V}sym\left(\nabla_0\Delta\mathbf{u}\cdot(\nabla_0\delta\mathbf{u})^{\mathrm{T}}\right):\mathbf{S}\mathrm{d}^0V + \int_{0V}sym(\nabla_0\delta\mathbf{u}):\mathbf{C}:sym(\nabla_0\Delta\mathbf{u})\mathrm{d}^0V=0 \tag{3}$$

Note that the stress $\mathbf{S}$ is defined independently of the reference frame after the linearization. Besides, the first integral in Eq. (3) reflects the stiffness term in linear systems, whereas the second one represents the geometric stiffness term found in buckling problems. The solution to Eq. (3) will be examined in detail in the solution procedure section, which will be transfomed into an eigenvalue issue.

2.2. Updated Lagrangian formulation

As an alternative, ULF describes structural deformation using the current configuration as the reference frame which facilitates the employment of rate-form-defined constitutive equations through using spatial tensors ($_t\mathbf{E}$, $_t\mathbf{S}$) rather than material tensors ($_0\mathbf{E}$, $_0\mathbf{S}$). Following this character, the associated variation equation can be written as:

$$\int_{tV}\delta_t^t\mathbf{E}:{}_t^t\mathbf{S}\mathrm{d}^tV=\delta L_{\text{ext}} \tag{4}$$

where ${}_t^t\mathbf{E}$ is the Eulerian strain tensor and ${}_t^t\mathbf{S}$ is the Cauchy stress tensor at time t. Their expressions are written as:

$$\begin{gathered}{}_t^t\mathbf{E}=\frac{1}{2}\left((\nabla\mathbf{u})^{\mathrm{T}}+\nabla\mathbf{u}+\nabla\mathbf{u}\cdot(\nabla\mathbf{u})^{\mathrm{T}}\right),\quad {}_t^tE_{ij}=\frac{1}{2}\left(\frac{\partial u_i}{\partial x_j}+\frac{\partial u_j}{\partial x_i}+\frac{\partial u_k}{\partial x_i}\frac{\partial u_k}{\partial x_j}\right)\quad i,\ j=1,2,3\\ \Delta_t\mathbf{S}^{\mathbf{J}}=\mathbf{C}:\Delta_t\mathbf{E},\quad \Delta_tS_{ij}=C_{ijkl}\ \Delta_tE_{kl}\quad i,\ j,\ k,\ l=1,2,3\end{gathered} \tag{5}$$

where the sign ∇ is the spatial gradient. $\Delta_t\mathbf{S}^{\mathbf{J}}$ represents the Jaumann incremental form of the Cauchy stress tensor, which is objective. Notably, the constitutive law in Eq. (5) must be given in the objective form to include the effect of rigid-body rotation. Besides, under the time-independent material coefficients hypothesis, $\Delta\mathbf{C}$ is not addressed in the rate-form constitutive law.

Typically, buckling analysis is performed on the initial geometry, Thus, in Eq. (4), the domain of the virtual work should be transformed into its undeformed configuration.

$$\int_{0V}\left((\nabla_0\delta\mathbf{u})\cdot(\nabla_0\mathbf{x})^{-1}\right):{}_t^t\mathbf{S}|J|\mathrm{d}^0V=\delta L_{\text{ext}} \tag{6}$$

where $\nabla_0\mathbf{x}$ is defined as the deformed gradient, and $|J|$ denotes its determinant. As a result, $|J|$ can be regarded as the amplification factor between the undeformed (d^0V) and deformed (d^tV) infinitesimal volumes. This denotation allows for the definition of a new stress measure called the Kirchhoff stress tensor in the undeformed area as $\boldsymbol{\tau}={}_t^t\mathbf{S}|J|$ conjugated to the Eulerian strain tensor, which has a clear physical meaning in contrast to the second Piola-Kirchhoff stress tensor conjugated to the Green-Lagrange strain tensor.

Due to the linearity of the strain–displacement relationship and constitutive law during the pre-buckling stage, it is unnecessary to distinguish between the second Piola-Kirchhoff, Cauchy, and Kirchhoff stresses, i.e., ${}_0^t\mathbf{S}\approx{}_t^t\mathbf{S}\approx\boldsymbol{\tau}$, as well as between material and spatial gradients, i.e., $\nabla_0\approx\nabla$ when the linearization is performed. Details on how these stresses are defined can be found in [49].

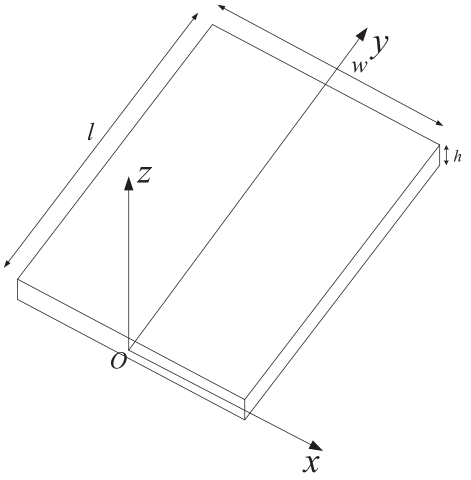

Figure 2. Cartesian coordinate system for a flat structure.

Taking the increment of Eq. (6), we obtain:

$$\begin{aligned}\Delta\left(\int_{{}^0V}(\nabla_0\delta\mathbf{u})\cdot(\nabla_0\mathbf{x})^{-1}:\boldsymbol{\tau}\mathrm{d}^0V\right)&=\int_{{}^0V}sym(\nabla_0\delta\mathbf{u}):\mathbf{C}:sym(\nabla_0\Delta\mathbf{u})\mathrm{d}^0V\\&+\int_{{}^0V}sym(\nabla_0\Delta\mathbf{u}\cdot(\nabla_0\delta\mathbf{u})^{\mathrm{T}}):\mathbf{S}\mathrm{d}^0V\\&-2\int_{{}^0V}\left(sym\left(\nabla_0\Delta\mathbf{u}\right)\cdot sym(\nabla_0\delta\mathbf{u})\right):\mathbf{S}\mathrm{d}^0V=0\end{aligned}\tag{7}$$

By comparing Eq. (7) and Eq. (3), it is obvious that ULF and TLF result in distinct buckling formulae. The additional term $2\int_{{}^0V}(sym(\nabla_0\Delta\mathbf{u})\cdot sym(\nabla_0\delta\mathbf{u})):\mathbf{S}\mathrm{d}^0V$ in Eq. (7) exemplifies this. Such a minute difference will be amplified if the related displacement gradient ($\nabla_0\delta\mathbf{u}$ or $\nabla_0\delta\mathbf{u}$ or $\nabla_0\mathbf{u}$) exhibits a considerable variation, as discussed later in the section on numerical results.

3. Structural model

3.1. Preliminary

The matrix–vector notation is more accessible for computer implementations of an in-house finite element code than the tensor notation. Consider a flat structure described in the Cartesian coordinate system and featured by its length l, the width w, and the thickness h, as illustrated in Figure 2. Vectors of displacement, strain, and stress can be expressed as follows in the case of linear thermoelasticity:

$$\begin{aligned}\mathbf{u}&=[u_x,u_y,u_z]^{\mathrm{T}}\\\boldsymbol{\varepsilon}&=[\varepsilon_{xx},\varepsilon_{yy},\varepsilon_{zz},\gamma_{xz},\gamma_{yz},\gamma_{xy}]^{\mathrm{T}}\\\mathbf{S}&=[S_{xx},S_{yy},S_{zz},S_{xz},S_{xz},S_{xy}]^{\mathrm{T}}\end{aligned}\tag{8}$$

Take note that $\boldsymbol{\varepsilon}$ is employed instead of $\mathbf{E}$ here due to the assumption of a small displacement gradient, and it is referred to as the engineering strain, as its shear component is twice that of the tensor. The geometrical relation and the constitutive equation take the following forms:

$$\begin{aligned}\boldsymbol{\varepsilon}&=\mathbf{D}\mathbf{u}\\\mathbf{S}&=\tilde{\mathbf{C}}(\boldsymbol{\varepsilon}-\boldsymbol{\varepsilon}^{th})\end{aligned}\tag{9}$$

where

$$\mathbf{D}=\begin{bmatrix}\frac{\partial}{\partial x} & 0 & 0\\ 0 & \frac{\partial}{\partial y} & 0\\ 0 & 0 & \frac{\partial}{\partial z}\\ \frac{\partial}{\partial z} & 0 & \frac{\partial}{\partial x}\\ 0 & \frac{\partial}{\partial z} & \frac{\partial}{\partial y}\\ \frac{\partial}{\partial y} & \frac{\partial}{\partial x} & 0\end{bmatrix},\tilde{\mathbf{C}}=\begin{bmatrix}\tilde{C}_{11} & \tilde{C}_{12} & \tilde{C}_{13} & 0 & 0 & \tilde{C}_{16}\\ \tilde{C}_{12} & \tilde{C}_{22} & \tilde{C}_{23} & 0 & 0 & \tilde{C}_{26}\\ \tilde{C}_{13} & \tilde{C}_{23} & \tilde{C}_{33} & 0 & 0 & \tilde{C}_{36}\\ 0 & 0 & 0 & \tilde{C}_{44} & \tilde{C}_{45} & 0\\ 0 & 0 & 0 & \tilde{C}_{45} & \tilde{C}_{55} & 0\\ \tilde{C}_{16} & \tilde{C}_{26} & \tilde{C}_{36} & 0 & 0 & \tilde{C}_{66}\end{bmatrix},\boldsymbol{\varepsilon}^{th}=\begin{bmatrix}\alpha_{xx}\Delta T\\ \alpha_{yy}\Delta T\\ \alpha_{zz}\Delta T\\ 0\\ 0\\ \alpha_{xy}\Delta T\end{bmatrix} \tag{10}$$

where the material stiffness matrix $\tilde{\mathbf{C}}$ is defined in the global coordinate system $[x,y,z]$, which is rotated to the material coordinate system $[1,2,3]$ by an angle θ for an orthotropic case. For clarity purposes, the components of $\tilde{\mathbf{C}}$ are not listed here; nonetheless, they maybe found be in [51]. $\boldsymbol{\varepsilon}^{th}$ is defined in the same way as $\boldsymbol{\varepsilon}$. A uniform temperature increase is assumed $(\Delta T \equiv constant)$ in the present work, and the thermal coefficient of expansion orientated at principal coordinate axis can be expressed as:

$$\begin{aligned}\alpha_{xx}&=(\alpha_{11}\cos^2\theta+\alpha_{22}\sin^2\theta)\\ \alpha_{yy}&=(\alpha_{11}\sin^2\theta+\alpha_{22}\cos^2\theta)\\ \alpha_{zz}&=\alpha_{33}\\ \alpha_{xy}&=2(\alpha_{11}-\alpha_{22})\sin\theta\cos\theta\end{aligned} \tag{11}$$

3.2. Carrera Unified Formulation (CUF)

CUF has been demonstrated to be applicable across a broad range of structural shapes and material properties [52]. The fundamental idea behind 1 D CUF is to define 3 D displacement vector as a cross-section expansion of 1 D displacement variables in the axial direction, with the explicit form being:

$$\mathbf{u}(x,y,z)=F_\tau(x,z)\mathbf{u}_\tau(y)\quad \tau=1,\ldots,M \tag{12}$$

where $\mathbf{u}_\tau(y)$ is the 1 D generalized displacement vector; the repeated subscript τ signifies summation in Einstein notation; and $F_\tau(x,z)$ is the function associated with the cross-section coordinate. Currently, under the CUF framework, both ESL and LW models can be constructed by selecting different types of expansion functions (TE, LE, CE, HLE, and IHLE). Among these, this work makes use of the IHLE beam theory.

3.2.1. Improved hierarchical Legendre expansion (IHLE)

IHLE, which Yan et al. [41,42] just developed, may be considered a derivation of HLE. It converts non-interpolative bases on the edge of HLE expansion domains to interpolative Lagrange-type nodal bases while maintaining hierarchical Legendre interpolation bases on the inside. As a result, before constructing IHLE, we will present an outline of HLE, which consists of vertex, side, and internal modes. For a quadrilateral domain with an inverval $[-1,1]\times[-1,1]$, their expressions are given as follows:

Vertex modes: they are used to characterize the deformation of four vertices over the quadrilateral plane.

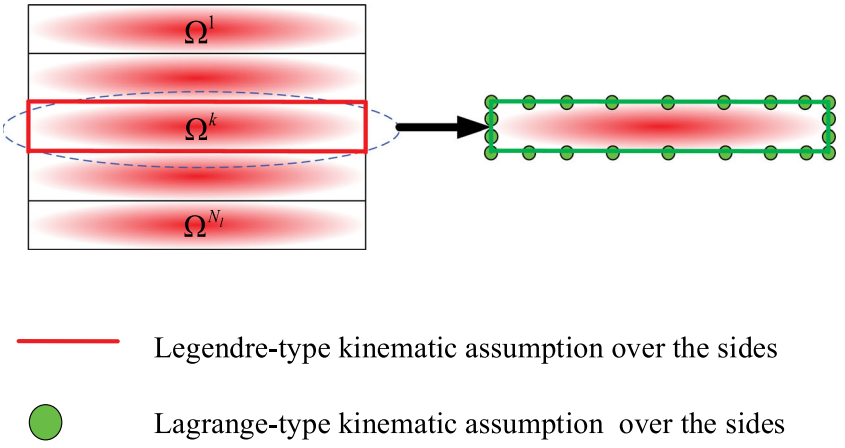

Figure 3. Transformation from HLE to IHLE.

$$F_\tau = \frac{1}{4}(1+\xi\ \xi_\tau)(1+\eta\ \eta_\tau); \qquad \tau = 1,2,3,4 \tag{13}$$

where ξ_τ and η_τ are the coordinates of point τ in the natural coordinate system. ξ and η range between [-1, +1].

Side modes: they are used to denote the edge-featuring deformation over the quadrilateral plane.

$$\begin{aligned}
F_\tau &= \frac{1}{2}(1-\eta)\phi_{j_1}(\xi); \qquad j_1 \geq 2; \qquad \tau = 5,9,13,18,\ldots \\
F_\tau &= \frac{1}{2}(1+\xi)\phi_{j_2}(\eta); \qquad j_2 \geq 2; \qquad \tau = 6,10,14,19,\ldots \\
F_\tau &= \frac{1}{2}(1+\eta)\phi_{j_3}(\xi); \qquad j_3 \geq 2; \qquad \tau = 7,11,15,20,\ldots \\
F_\tau &= \frac{1}{2}(1-\xi)\phi_{j_4}(\eta); \qquad j_4 \geq 2; \qquad \tau = 8,12,16,21,\ldots
\end{aligned} \tag{14}$$

where $j_i; \quad i = 1,2,3,4$ is the expansion order of the ith edge. ϕ_{j_i} is the integrated Legendre polynomial, which is described in depth in [53].

Internal modes: they are used to illustrate the deformation that happens on the internal face and vanishes at nodes and edges.

$$F_\tau = \phi_{j_m}(\xi)\phi_{k_n}(\eta); \qquad j_m,\ k_n \geq 2; \qquad m,\ n = 1,2,3,4; \qquad \tau = 17,22,23,28,29,30\cdots \tag{15}$$

It should be noted that, with the exception of the kinematic terms referring to vertex modes, the remainder of the kinematic ones related to side and internal modes lack a clear physical meaning. When the complicated (arbitrary-shaped) cross-section are discretized into an optional number of quadrilateral sub-domains, the assembly of terms in adjacent sub-domains becomes difficult. Besides, the expansion order of side and internal modes is unrelated, laying the groundwork for the IHLE implementation.

Figure 3 specifies the transformation of the expansion function over the side in the kth subdomain. Assume that $\mathbf{u}_\tau^{\mathrm{g}}(y) = \left[u_{x_\tau}^{\mathrm{g}}, u_{y_\tau}^{\mathrm{g}}, u_{z_\tau}^{\mathrm{g}}\right]^{\mathrm{T}}$ is the displacement vector related to the τth Gauss-Lobatto node (ξ_τ, η_τ) with the total number N. Due to the fact that three components of displacement fields have an equal amount of expansion terms, we will illustrate the detailed process by taking the component along the x direction as an example.

$$\boldsymbol{U}_x^{\mathrm{g}} = \mathbf{V}\boldsymbol{U}_x \tag{16}$$

where

$$\mathbf{V} = \begin{bmatrix} F_1(\xi_1,\eta_1) & \cdots & F_\tau(\xi_1,\eta_1) & \cdots & F_N(\xi_1,\eta_1) \\ \cdots & \cdots & \cdots & \cdots & \cdots \\ F_1(\xi_\tau,\eta_\tau) & \ldots & F_\tau(\xi_\tau,\eta_\tau) & \ldots & F_N(\xi_\tau,\eta_\tau) \\ \cdots & \cdots & \cdots & \cdots & \cdots \\ F_1(\xi_N,\eta_N) & \ldots & F_\tau(\xi_N,\eta_N) & \ldots & F_N(\xi_N,\eta_N) \end{bmatrix} \quad \begin{matrix} \boldsymbol{U}_x^{\mathrm{g}} = \left[u_{x_1}^{\mathrm{g}},\ldots,u_{x_\tau}^{\mathrm{g}},\ldots,u_{x_N}^{\mathrm{g}}\right]^{\mathrm{T}} \\ \\ \\ \\ \boldsymbol{U}_x = \left[u_{x_1},\ldots,u_{x_\tau},\ldots,u_{x_N}\right]^{\mathrm{T}} \end{matrix} \tag{17}$$

Additionally, the total number of transformed nodes must equal that of the expansion terms relative to vertex and side modes. Due to the mathematical constraint, the nodal collocation technique is such that non-equispaced nodes, especially Gauss-Lobatto nodes, are chosen for each edge in order to mitigate the significant oscillation problem associated with a growing number of nodes, referred to as Runge's phenomenon.

The local displacement field of four edges (including four vertices), indicated by $\mathbf{u}_x^{\mathrm{fes}}(x,y,z)$, can be expressed in terms of nodal displacement variables using the relation in Eq. (16):

$$\begin{aligned} \mathbf{u}_x^{\mathrm{fes}} &= L_\tau(\xi,\eta)\mathbf{u}_{x_\tau}^{\mathrm{g}}(y) \\ \boldsymbol{L} &= \mathbf{G}\mathbf{V}^{-1} \end{aligned} \tag{18}$$

where $\mathbf{G} = [F_1, F_2, ..., F_N]$ is the vectorization representation of the expansion function $F_\tau(\xi,\eta)$; $\tau = 1,2,....,N$; L_τ means the Lagrange-type interpolation function and its vectorized form is denoted by $\boldsymbol{L}$.

Bear in mind that the transformation occurring on the edge has no effect on the Legendre-like kinematics within the sub-domain. This critical property enables the formulation of a novel kinematic field, which asserts that:

$$\begin{aligned} \mathbf{u} &= L_{\tau_1}(\xi,\eta)\mathbf{u}_{\tau_1}^{\mathrm{g}}(y) + F_{\tau_2}(\xi,\eta)\mathbf{u}_{\tau_2}(y); \quad \tau_1 = 1,2,...,N; \quad \tau_2 = 1,2,...,M-N; \quad \tau_1 \neq \tau_2 \\ &= \bar{F}_\tau(\xi,\eta)\mathbf{u}_\tau(y); \quad \tau = 1,2,...,M \end{aligned} \tag{19}$$

where $\bar{F}(\xi,\eta)$ is the IHLE-type kinematic assumption, which is a combination of Lagrange and hierarchical Legendre expansions.

The key feature of this variable-kinematic beam model is that the degrees of freedom on the border of the cross-section have a clear physical meaning (see Figure 3). Thus, the implementation of LW models can be done in a straightforward manner. In other words, through the assembly of coinciding degrees of freedom, the continuity of displacements at the plies' interfaces is imposed. The discussion of LW theories is out of the scope of this paper, but the reader can refer to the literature [44]. Besides, the basis transformation acting exclusively on edges preserves the partial hierarchical properties of the original HLE model. In other words, kinematic refinement can still be simply accomplished by adjusting the polynomial order. The effectiveness of the additional but essential transformation is dependent on the time consumed by the matrix inversion in Eq. (18).

The traditional FE formulation is widely utilized to address mechanical problems due to its simplicity and broad application. In the present work, the standard 1 D shape function N_i in FEM is selected to interpolate the axial displacement variable $\mathbf{u}_\tau$

$$\mathbf{u}_\tau(y) = N_i(y)\mathbf{q}_{\tau i} \quad i = 1,...,n \tag{20}$$

where $\mathbf{q}_{\tau i}$ is a nodal unknown vector; and n denotes the number of nodes contained within an element. Four-node (B4) Lagrange-type element is chosen in this work with the following expression:

$$N_i(\gamma) = \frac{\prod_{j=1}^{4}(\gamma - \gamma_j)}{\prod_{j=1,j\neq i}^{4}(\gamma_i - \gamma_j)} \tag{21}$$

where N_i is specified in the isoparametric space $[-1,1]$ with the equidistant root γ_i. Accordingly, under the framework of CUF-based FEM approximation, the complement expression of 3 D displacement field is as follows:

$$\mathbf{u}(x,y,z) = \bar{F}_\tau(x,z)N_i(y)\mathbf{q}_{\tau i} \quad i = 1,\ldots,n \tag{22}$$

4. Solution procedure

The buckling problem can be transformed mathematically into a generalized eigenvalue problem. However, as seen from the governing equations (Eq. (7) and Eq. (3)) to be discretized, the solution process is strongly dependent on the distribution of displacement and temperature changes at the pre-buckling stage. In certain specialized cases, such as thin symmetric laminates or thin isotropic panels with four edges that are either fully clamped or simply-supported, 3 D thermal buckling problems can be reduced to in-plane buckling problems under the assumption of uniform temperature changes. The pre-buckling strain ($\boldsymbol{\varepsilon}$) is equal to zero in this circumstance, and the pre-buckling stress is mostly caused by thermal strain ($\boldsymbol{\varepsilon}^{th}$, see Eq. 9). Thus, eigenvalue analysis alone can be used to calculate the critical temperature, resulting in what is known as one-step analysis. Otherwise, prior to performing the eigenvalue analysis, the pre-buckling strain should be calculated. For convenience, we'll refer to this type of solution technique as two-step analysis, which will be presented immediately without any loss of generality.

4.1. Two-step analysis

Because pre-buckling analysis is restricted to the small strain assumption, no distinction is possible between Eq. (1) and Eq. (4). By substitution of Eq. (9), Eq. (19), Eq. (12), and Eq. (20) into Eq. (1), we can obtain the governing equation of linear thermoelastic problem in a discretization manner:

$$\mathbf{K}\mathbf{q} = \mathbf{P}^{th} \tag{23}$$

where $\mathbf{K}$ is denoted as the stiffness matrix containing the fundamental nucleus (FN) of dimension 3×3:

$$\begin{aligned}
K^{\tau sij}[1,1] &= \left(E^{11}_{\tau,_x s,_x} + E^{44}_{\tau,_z s,_z}\right)J_{ij} + E^{16}_{\tau,_x s}J_{ij,_y} + E^{16}_{\tau s,_x}J_{i,_y j} + E^{66}_{\tau s}J_{i,_y j,_y}\\
K^{\tau sij}[1,2] &= \left(E^{16}_{\tau,_x s,_x} + E^{45}_{\tau,_z s,_z}\right)J_{ij} + E^{12}_{\tau,_x s}J_{ij,_y} + E^{66}_{\tau s,_x}J_{i,_y}j + E^{26}_{\tau s}J_{i,_y}j,_y\\
K^{\tau sij}[1,3] &= \left(E^{13}_{\tau,_x s,_z} + E^{44}_{\tau,_z s,_x}\right)J_{ij} + E^{45}_{\tau,_z s}J_{ij,_y} + E^{36}_{\tau s,_z}J_{i,_y j}\\
K^{\tau sij}[2,1] &= \left(E^{16}_{\tau,_x s,_x} + E^{45}_{\tau,_z s,_z}\right)J_{ij} + E^{66}_{\tau,_x s}J_{ij,_y} + E^{12}_{\tau s,_x}J_{i,_y}j + E^{26}_{\tau s}J_{i,_y j,_y}\\
K^{\tau sij}[2,2] &= \left(E^{66}_{\tau,_x s,_x} + E^{55}_{\tau,_z s,_z}\right)J_{ij} + E^{26}_{\tau,_x s}J_{ij,_y} + E^{26}_{\tau s,_x}J_{i,_y}j + E^{22}_{\tau s}J_{i,_y}j,_y\\
K^{\tau sij}[2,3] &= \left(E^{36}_{\tau,_x s,_z} + E^{45}_{\tau,_z s,_x}\right)J_{ij} + E^{55}_{\tau,_z s}J_{ij,_y} + E^{23}_{\tau s,_z}J_{i,_y j}\\
K^{\tau sij}[3,1] &= \left(E^{44}_{\tau,_x s,_z} + E^{13}_{\tau,_z s,_x}\right)J_{ij} + E^{36}_{\tau,_z s}J_{ij,_y} + E^{45}_{\tau s,_z}J_{i,_y j}\\
K^{\tau sij}[3,2] &= \left(E^{45}_{\tau,_x s,_z} + E^{36}_{\tau,_z s,_x}\right)J_{ij} + E^{23}_{\tau,_z s}J_{ij,_y} + E^{55}_{\tau s,_z}J_{i,_y j}\\
K^{\tau sij}[3,3] &= \left(E^{44}_{\tau,_x s,_x} + E^{33}_{\tau,_z s,_z}\right)J_{ij} + E^{45}_{\tau,_x s}J_{ij,_y} + E^{45}_{\tau s,_x}J_{i,_y j} + E^{55}_{\tau s}J_{i,_y j,_y}
\end{aligned} \tag{24}$$

where the terms $E^{\alpha\beta}_{\tau,_\theta s,_\zeta}$ and $J_{i,_\xi j,_\varsigma}$ denote the cross-section moment parameter and integral along the beam axis, respectively, as follows:

$$E^{\alpha\beta}_{\tau,_{\theta}s,_{\zeta}} = \int_{\Omega} \tilde{C}_{\alpha\beta}\bar{F}_{\tau,_{\theta}}(x,z)\bar{F}_{s,_{\zeta}}(x,z)\mathrm{d}\Omega$$
$$J_{i,_{\zeta}j,_{\varsigma}} = \int_{L} N_{i,_{\zeta}}(y)N_{j,_{\varsigma}}(y)\mathrm{d}y \tag{25}$$

Due to the absence of the mechanical load, the nodal loading vector refers to the thermally induced part ($\mathbf{P}^{th}$), whose FN ($\mathbf{P}^{th}_{\tau i}$) consists of a 3×1 vector:

$$\begin{aligned}
P^{th}_{\tau i}[1,1] &= \alpha_{yy}\Delta T_0(E^{12}_{\tau,_x}J_i + E^{26}_{\tau}J_{i,_y}) + \alpha_{xx}\Delta T_0(E^{11}_{\tau,_x}J_i + E^{16}_{\tau}J_{i,_y}) + \alpha_{zz}\Delta T_0(E^{13}_{\tau,_x}J_i + E^{36}_{\tau}J_{i,_y}) + \alpha_{xy}\Delta T_0(E^{16}_{\tau,_x}J_i + E^{66}_{\tau}J_{i,_y})\\
P^{th}_{\tau i}[2,1] &= \alpha_{yy}\Delta T_0(E^{22}_{\tau}J_{i,_y} + E^{26}_{\tau,_x}J_i) + \alpha_{xx}\Delta T_0(E^{12}_{\tau}J_{i,_y} + E^{16}_{\tau,_x}J_i) + \alpha_{zz}\Delta T_0(E^{23}_{\tau}J_{i,_y} + E^{36}_{\tau,_x}J_i) + \alpha_{xy}\Delta T_0(E^{26}_{\tau}J_{i,_y} + E^{66}_{\tau,_x}J_i)\\
P^{th}_{\tau i}[3,1] &= \alpha_{yy}\Delta T_0(E^{23}_{\tau,_z}J_i) + \alpha_{xx}\Delta T_0(E^{13}_{\tau,_z}J_i) + \alpha_{zz}\Delta T_0(E^{33}_{\tau,_z}J_i) + \alpha_{xy}\Delta T_0(E^{36}_{\tau,_z}J_i)
\end{aligned} \tag{26}$$

ΔT_0 is the reference temperature change. Notably, the generated FNs are invariant, which means that their expression remains constant regardless of the shape or cross-section expansion function used. Additionally, integrals are decoupled throughout the cross-section and along the beam axis. Thus, classical and higher-order beam theories can be constructed by appropriately raising the order of the expansion function without regard for the element size in the longitudinal direction; consequently, there are no aspect ratio limitations between these two domains.

FN is often limited to the cross-section sub-domain of a single 1 D CUF finite element in the LW model. The global stiffness matrix can be constructed by expanding the indices τ, s, i, and j. Interesting readers might consult the literature [33] for a more complete implementation. After obtaining global matrices, it is possible to solve a system of linear algebraic equations by imposition of boundary conditions.

After obtaining the pre-buckling displacement, the corresponding stress ($\mathbf{S}$) can be determined using the constitutive equation. Bifurcation points (typical of buckling) connected with the current equilibrium state appear when the tangent stiffness matrix ($\mathbf{K}_T$) has a zero determinant, i.e.,

$$|\mathbf{K}_T| = |\mathbf{K} + \lambda_{cr}\mathbf{K}_g| = 0 \tag{27}$$

where $\mathbf{K}$ is the stiffness matrix with the same FN as in Eq. (24); λ_{cr} is the eigenvalue, which is multiplied by the reference temperature change ΔT_0 to get the critical value. $\mathbf{K}_g$ is the geometric stiffness matrix related to $\mathbf{S}$. FN in $\mathbf{K}_g$, on the other hand, takes on a separate form in TLF and ULF, depending on the reference frame used.

Substituting Eq. (9), Eq. (19), Eq. (12), and Eq. (20) into Eq. (3) yields FN ($K^{\tau sij}_g$) in TLF as:

$$K^{\tau sij}_g[:,:] = D^{\tau sij}\mathbf{I} \tag{28}$$

in which

$$\begin{aligned}
D^{\tau sij} = &< S_{xx}\bar{F}_{\tau,_x}\bar{F}_{s,_x}N_iN_j > + < S_{yy}\bar{F}_{\tau}\bar{F}_{s}N_{i,_y}N_{j,_y} > + < S_{zz}\bar{F}_{\tau,_z}\bar{F}_{s,_z}N_iN_j >\\
&+ < S_{xy}\bar{F}_{\tau,_x}\bar{F}_{s}N_iN_{j,_y} > + < S_{xy}\bar{F}_{\tau}\bar{F}_{s,_x}N_{i,_y}N_j > + < S_{xz}\bar{F}_{\tau,_x}\bar{F}_{s,_z}N_iN_j >\\
&+ < S_{xz}\bar{F}_{\tau,_z}\bar{F}_{s,_x}N_iN_j > + < S_{yz}\bar{F}_{\tau,_z}\bar{F}_{s}N_iN_{j,_y} > + < S_{yz}\bar{F}_{\tau}\bar{F}_{s,_z}N_{i,_y}N_j) >
\end{aligned} \tag{29}$$

where $\mathbf{I}$ is the 3×3 identity matrix; and $< (\cdot) >= \int_{_0V} (\cdot)\mathrm{d}^0V$. Different from the diagonal form, FN ($K^{\tau sij}_g$) in ULF takes the full form by inserting Eq. (9), Eq. (19), Eq. (12), and Eq. (20) into Eq. (7):

$$
\begin{aligned}
K_g^{\tau sij}[1,1] = \; & D^{\tau sij} - 2 < S_{xx}\bar{F}_{\tau,_x}\bar{F}_{s,_x}N_iN_j > - \frac{1}{2} < S_{xx}\bar{F}_{\tau}\bar{F}_sN_{i,_y}N_{j,_y} > - \frac{1}{2} < S_{xx}\bar{F}_{\tau,_z}\bar{F}_{s,_z}N_iN_j > \\
& - \frac{1}{2} < S_{yy}\bar{F}_{\tau}\bar{F}_sN_{i,_y}N_{j,_y} > - \frac{1}{2} < S_{zz}\bar{F}_{\tau,_z}\bar{F}_{s,_z}N_iN_j > - < S_{xy}\bar{F}_{\tau}\bar{F}_{s,_x}N_{i,_y}N_j > - < S_{xy}\bar{F}_{\tau,_x}\bar{F}_sN_iN_{j,_y} > \\
& - < S_{xz}\bar{F}_{\tau,_x}\bar{F}_{s,_z}N_iN_j > - < S_{xz}\bar{F}_{\tau,_z}\bar{F}_{s,_x}N_iN_j > - \frac{1}{2} < S_{yz}\bar{F}_{\tau,_z}\bar{F}_sN_iN_{j,_y} > - \frac{1}{2} < S_{yz}\bar{F}_{\tau}\bar{F}_{s,_z}N_{i,_y}N_j > \\
K_g^{\tau sij}[1,2] = \; & - \frac{1}{2} < S_{xx}\bar{F}_{\tau}\bar{F}_{s,_x}N_{i,_y}N_j > - \frac{1}{2} < S_{yy}\bar{F}_{\tau}\bar{F}_{s,_x}N_{i,_y}N_j > - < S_{xy}\bar{F}_{\tau,_x}\bar{F}_{s,_x}N_iN_j > \\
& - < S_{xy}\bar{F}_{\tau}\bar{F}_sN_{i,_y}N_{j,_y} > - \frac{1}{2} < S_{xy}\bar{F}_{\tau,_z}\bar{F}_{s,_z}N_iN_j > - \frac{1}{2} < S_{xz}\bar{F}_{\tau}\bar{F}_{s,_z}N_{i,_y}N_j > - \frac{1}{2} < S_{yz}\bar{F}_{\tau,_z}\bar{F}_{s,_x}N_iN_j > \\
K_g^{\tau sij}[1,3] = \; & - \frac{1}{2} < S_{xx}\bar{F}_{\tau,_z}\bar{F}_{s,_x}N_iN_j > - \frac{1}{2} < S_{zz}\bar{F}_{\tau,_z}\bar{F}_{s,_x}N_iN_j > - \frac{1}{2} < S_{xy}\bar{F}_{\tau,_z}\bar{F}_sN_iN_{j,_y} > \\
& - < S_{xz}\bar{F}_{\tau,_x}\bar{F}_{s,_x}N_iN_j > - \frac{1}{2} < S_{xz}\bar{F}_{\tau}\bar{F}_sN_{i,_y}N_{j,_y} > - < S_{xz}\bar{F}_{\tau,_z}\bar{F}_{s,_z}N_iN_j > - \frac{1}{2} < S_{yz}\bar{F}_{\tau}\bar{F}_{s,_x}N_{i,_y}N_j > \\
K_g^{\tau sij}[2,1] = \; & - \frac{1}{2} < S_{xx}\bar{F}_{\tau,_x}\bar{F}_sN_iN_{j,_y} > - \frac{1}{2} < S_{yy}\bar{F}_{\tau,_x}\bar{F}_sN_iN_{j,_y} > - < S_{xy}\bar{F}_{\tau,_x}\bar{F}_{s,_x}N_iN_j > \\
& - < S_{xy}\bar{F}_{\tau}\bar{F}_sN_{i,_y}N_{j,_y} > - \frac{1}{2} < S_{xy}\bar{F}_{\tau,_z}\bar{F}_{s,_z}N_iN_j > - \frac{1}{2} < S_{xz}\bar{F}_{\tau,_z}\bar{F}_sN_iN_{j,_y} > - \frac{1}{2} < S_{yz}\bar{F}_{\tau,_x}\bar{F}_{s,_z}N_iN_j > \\
K_g^{\tau sij}[2,2] = \; & D^{\tau sij} - \frac{1}{2} < S_{xx}\bar{F}_{\tau,_x}\bar{F}_{s,_x}N_iN_j > - \frac{1}{2} < S_{yy}\bar{F}_{\tau,_x}\bar{F}_{s,_x}N_iN_j > - 2 < S_{yy}\bar{F}_{\tau}\bar{F}_sN_{i,_y}N_{j,_y} > \\
& - \frac{1}{2} < S_{yy}\bar{F}_{\tau,_z}\bar{F}_{s,_z}N_iN_j > - \frac{1}{2} < S_{zz}\bar{F}_{\tau,_z}\bar{F}_{s,_z}N_iN_j > - < S_{xy}\bar{F}_{\tau}\bar{F}_{s,_x}N_{i,_y}N_j > - < S_{xy}\bar{F}_{\tau,_x}\bar{F}_sN_iN_{j,_y} > \\
& - \frac{1}{2} < S_{xz}\bar{F}_{\tau,_x}\bar{F}_{s,_z}N_iN_j > - \frac{1}{2} < S_{xz}\bar{F}_{\tau,_z}\bar{F}_{s,_x}N_iN_j > - < S_{yz}\bar{F}_{\tau,_z}\bar{F}_sN_iN_{j,_y} > - < S_{yz}\bar{F}_{\tau}\bar{F}_{s,_z}N_{i,_y}N_j > \\
K_g^{\tau sij}[2,3] = \; & - \frac{1}{2} < S_{yy}\bar{F}_{\tau,_z}\bar{F}_sN_iN_{j,_y} > - \frac{1}{2} < S_{zz}\bar{F}_{\tau,_z}\bar{F}_sN_iN_{j,_y} > - \frac{1}{2} < S_{xy}\bar{F}_{\tau,_z}\bar{F}_{s,_x}N_iN_j > \\
& - \frac{1}{2} < S_{xz}\bar{F}_{\tau,_x}\bar{F}_sN_iN_{j,_y} > - \frac{1}{2} < S_{yz}\bar{F}_{\tau,_x}\bar{F}_{s,_x}N_iN_j > - < S_{yz}\bar{F}_{\tau}\bar{F}_sN_{i,_y}N_{j,_y} > - < S_{yz}\bar{F}_{\tau,_z}\bar{F}_{s,_z}N_iN_j > \\
K_g^{\tau sij}[3,1] = \; & - \frac{1}{2} < S_{xx}\bar{F}_{\tau,_x}\bar{F}_{s,_z}N_iN_j > - \frac{1}{2} < S_{zz}\bar{F}_{\tau,_x}\bar{F}_{s,_z}N_iN_j > - \frac{1}{2} < S_{xy}\bar{F}_{\tau}\bar{F}_{s,_z}N_{i,_y}N_{j,_y} > \\
& - < S_{xz}\bar{F}_{\tau,_x}\bar{F}_{s,_x}N_iN_j > - \frac{1}{2} < S_{xz}\bar{F}_{\tau}\bar{F}_sN_{i,_y}N_{j,_y} > - < S_{xz}\bar{F}_{\tau,_z}\bar{F}_{s,_z}N_iN_j > - \frac{1}{2} < S_{yz}\bar{F}_{\tau,_x}\bar{F}_sN_iN_{j,_y} > \\
K_g^{\tau sij}[3,2] = \; & - \frac{1}{2} < S_{yy}\bar{F}_{\tau}\bar{F}_{s,_z}N_{i,_y}N_j > - \frac{1}{2} < S_{zz}\bar{F}_{\tau}\bar{F}_{s,_z}N_{i,_y}N_j > - \frac{1}{2} < S_{xy}\bar{F}_{\tau,_x}\bar{F}_{s,_z}N_iN_j > \\
& - \frac{1}{2} < S_{xz}\bar{F}_{\tau}\bar{F}_{s,_x}N_{i,_y}N_j > - \frac{1}{2} < S_{yz}\bar{F}_{\tau,_x}\bar{F}_{s,_x}N_iN_j > - < S_{yz}\bar{F}_{\tau}\bar{F}_sN_{i,_y}N_{j,_y} > - < S_{yz}\bar{F}_{\tau,_z}\bar{F}_{s,_z}N_iN_j > \\
K_g^{\tau sij}[3,3] = \; & D^{\tau sij} - \frac{1}{2} < S_{xx}\bar{F}_{\tau,_x}\bar{F}_{s,_x}N_iN_j > - \frac{1}{2} < S_{yy}\bar{F}_{\tau}\bar{F}_sN_{i,_y}N_{j,_y} > - \frac{1}{2} < S_{zz}\bar{F}_{\tau,_x}\bar{F}_{s,_x}N_iN_j > \\
& - \frac{1}{2} < S_{zz}\bar{F}_{\tau}\bar{F}_sN_{i,_y}N_{j,_y} > - 2 < S_{zz}\bar{F}_{\tau,_z}\bar{F}_{s,_z}N_iN_j > - \frac{1}{2} < S_{xy}\bar{F}_{\tau}\bar{F}_{s,_x}N_{i,_y}N_j > - \frac{1}{2} < S_{xy}\bar{F}_{\tau,_x}\bar{F}_sN_iN_{j,_y} > \\
& - < S_{xz}\bar{F}_{\tau,_x}\bar{F}_{s,_z}N_iN_j > - < S_{xz}\bar{F}_{\tau,_z}\bar{F}_{s,_x}N_iN_j > - < S_{yz}\bar{F}_{\tau,_z}\bar{F}_sN_iN_{j,_y} > - < S_{yz}\bar{F}_{\tau}\bar{F}_{s,_z}N_{i,_y}N_j >
\end{aligned}
\tag{30}
$$

ULF, as comparison to TLF, contains redundant terms, which occur as a result of the degeneracy of the current geometry into the reference geometry. When geometrical nonlinear deformation increases, their effect is amplified. As with the stiffness matrix, the 3×3 FN can be utilized as the fundamental building block for constructing the geometric stiffness matrix for any higher-order refined beam element accounting for varied kinematics. In summary, the solution process in terms of two-step analysis can be written in a compact form as:

$$
\begin{cases}
\mathbf{Kq} = \mathbf{P}^{th} \\
\left|\mathbf{K} + \lambda_{cr}\mathbf{K}_g\right| = 0
\end{cases}
\tag{31}
$$

4.2. One-step analysis

The first step toward implementing one-step analysis is to set the thermal stress caused by the thermal strain to zero across the thickness, hence reducing to the in-plane stress problem. The specific strategy is to alter the elastic coefficients anchored on the thermal strain. The modified elastic coefficients in the material coordinate system are listed as follows:

$$C_{11}^{new} = \frac{E_1}{1 - \nu_{12}\nu_{21}}, C_{12}^{new} = \frac{\nu_{21}E_2}{1 - \nu_{12}\nu_{21}}, C_{22}^{new} = \frac{E_2}{1 - \nu_{12}\nu_{21}} \tag{32}$$

Accordingly, the constitutive law given by Eq. (9) may then be recast into the alternative form:

$$\mathbf{S} = \tilde{\mathbf{C}}\boldsymbol{\varepsilon} - \tilde{\mathbf{C}}^{new}\boldsymbol{\varepsilon}^{th} \tag{33}$$

where

$$\tilde{\mathbf{C}}^{new} = \begin{bmatrix} \tilde{C}_{11}^{new} & \tilde{C}_{12}^{new} & 0 & 0 & 0 & \tilde{C}_{16}^{new} \\ \tilde{C}_{12}^{new} & \tilde{C}_{22}^{new} & 0 & 0 & 0 & \tilde{C}_{26}^{new} \\ 0 & 0 & 0 & 0 & 0 & 0 \\ 0 & 0 & 0 & 0 & 0 & 0 \\ 0 & 0 & 0 & 0 & 0 & 0 \\ \tilde{C}_{16}^{new} & \tilde{C}_{26}^{new} & 0 & 0 & 0 & \tilde{C}_{66}^{new} \end{bmatrix} \tag{34}$$

where $\tilde{\mathbf{C}}^{new}$ is defined in the global coordinate system, the components of which are transformed from the terms $(C_{11}^{new}, C_{22}^{new}, C_{12}^{new})$ in the material coordinate system. Detailed expression can be found in Reddy [54].

Another fundamental justification for one-step analysis is that the strain response (both in-plane and out-of-plane) caused by the temperature change during the pre-buckling stage is irrelevant. Then, substituting the new relation $\mathbf{S} = -\tilde{\mathbf{C}}^{new}\boldsymbol{\varepsilon}^{th}$ into Eq. (3), we can just do the eigenvalue analysis described in the second equation of Eq. (31) to get the critical temperature. It should be pointed out the expression for FN in one-step analysis is identical to that in two-step analysis, which will be omitted for brevity.

5. Numerical results

Numerous numerical examples involving beam and plate structures are used to demonstrate the correctness and versatility of the proposed CUF-IHLE model. The first case is related to the thermal buckling behavior of metallic beams with a range of thickness-to-length ratios, with an emphasis on comparisons between various models, including ABAQUS 2 D, ABAQUS 3 D, IHLE-TLF, and IHLE-ULF. Note that ABAQUS results are based on ULF. Following that, the same comparison investigation is conducted on laminated beams. The role of shear and normal deformations is further explored. The final case examines the capabilities of one-step analysis in the thermal buckling problem of the laminated plates with zero-displacement boundary conditions, discussing the effect of the fiber orientation angle and thickness-to-length ratio, and providing the solutions obtained through two-step analysis for comparison purposes.

5.1. Metallic beam

The critical thermal solutions of metallic beams with a square cross-section are addressed in the preliminary validation. A set of thickness-to-length ratios (h/l) is taken into account while the length is kept constant ($l = 1$ m). The studied structure is composed of aluminum alloy materials being Young modulus $E = 72$ GPa, Poisson ratio $\nu = 0.33$, and the coefficient of thermal expansion $\alpha = 23 \times 10^{-6}/^{\circ}\mathrm{C}$. Boundary conditions of clamped types are assumed at both ends, as shown in Figure 4.

Table 1 shows the convergence property of the first buckling values with respect to the number and type of elements along the axial direction and the kinematic order over the cross-section used in the FEM-based CUF models. A group of 2 D and 3 D finite element solutions obtained via the commercial software Abaqus is presented here for comparison purposes. Due to their insensitivity to shear locking, the quadratic shell element with reduced integration scheme (S8R)

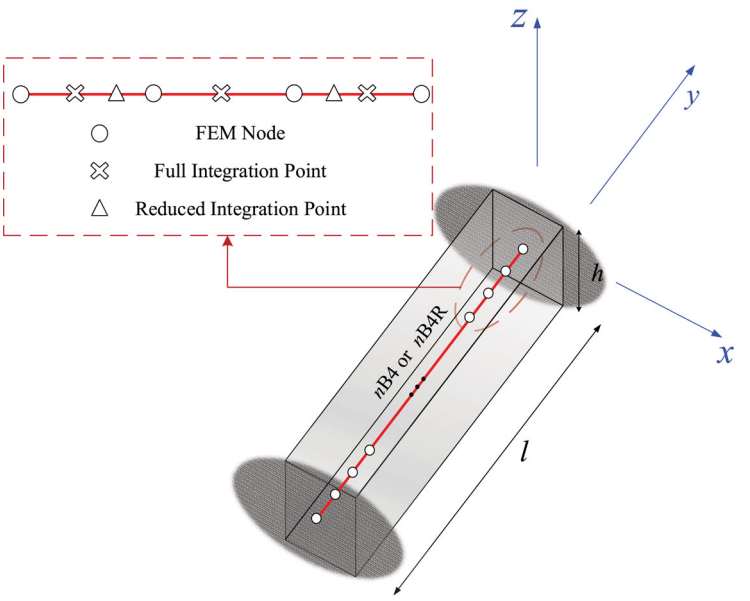

Figure 4. Geometric properties, boundary condition, and FEM discretization of the metallic beam.

and quadratic brick element with full and reduced integration schemes (C3D20 or C3D20R) are used in particular. Among them, the letter" R" means the reduced integration scheme. On the other hand, 1 D CUF-IHLE-based beam elements are indicated by the notation ϑB4R + 1IHL$\xi \times \zeta$ with the reduced integration scheme working exclusively on the axial direction (see Figure 4), where ϑ refers to the number of cubic beam elements, and ξ and ζ stand for the kinematic order along the x and z direction. The degree of freedom (DOF) is listed in the last column of the table.

By observing numerical results provided by various approaches, it can be found that the method implemented within the framework of IHLE-ULF is able to lead to correct values at the lower computational consumption. The results computed by IHLE-TLF and S8R models reach smaller values than those by the corresponding IHLE-ULF and C3D20 (R) models for $h/l > 0.01$, and S8R and IHLE-TLF models fails for $h/l \geq 0.1$. By comparison of Eq. (28) and Eq. (30), the discrepancy between the IHLE-TLF and -ULF model stems from diagonal and off-diagonal terms with negative values. While regarding the difference between S8R and C3D20R models, different kinematic assumptions through the thickness account for the underlying reason. In the case of $h/l = 0.01$, the beam is less affected by the transverse shear deformation, resulting in the close values between refined S8R and C3D20R results, at least to two significant digits. The C3D20 model predicts lower values in comparison to its reduced integration form constantly. Such a difference can be insignificant for a comparatively thicker beam. The fundamental reason is that when h/l is relatively small, the C3D20 soltion is marginally influenced by the shear locking, which can be overcome by the associated reduced integration scheme. Note that the behavior of the locking-insensitive solutions may not show a decreasing trend with the refinement of the element on a whole range of h/l. In general, increasing values can be seen with respect to the type of the S8R element, yet C3D20R follows the opposite trend with the exception of h/l equal to 0.06 and 0.08. On the contrary, IHLE results yield a monotonic increase with the augment of beam elements except for $h/l = 0.20$ but an analogous decrease with higher-order kinematics.

Table 1. Convergence of the thermal buckling loads of metallic beams for various thickness-to-length ratios.

	h/l						
Model	**0.01**	**0.06**	**0.08**	**0.10**	**0.15**	**0.20**	DOF
Abaqus-S8R[a]	14.274	493.55	852.16	1284.3	2573.6	3966.0	1950
Abaqus-S8R[b]	14.274	493.88	852.83	1285.4	2576.1	3970.0	3342
Abaqus-C3D20R[c]	14.281	496.82	864.18	1315.5	2727.2	4383.1	3663
Abaqus-C3D20R[d]	14.271	496.87	864.28	1315.5	2724.9	4375.0	8520
Abaqus-C3D20[d]	14.247	496.80	864.18	1315.3	2724.3	4373.9	8520
IHLE-TLF							
10B4R + 1IHL2 × 2	14.231	487.03	835.57	1250.7	2464.7	3746.5	744
15B4R + 1IHL2 × 2	14.251	487.29	835.92	1251.1	2465.0	3746.4	1104
20B4R + 1IHL2 × 2	14.254	487.32	835.96	1251.2	2465.0	3746.2	1464
20B4R + 1IHL3 × 3	14.254	485.95	831.49	1240.7	2424.0	3655.1	2379
20B4 + 1IHL3 × 3	14.218	485.64	831.03	1240.1	2423.3	3654.6	2379
IHLE-ULF							
10B4R + 1IHL2 × 2	14.240	498.31	869.69	1329.9	2790.9	4554.5	744
15B4R + 1IHL2 × 2	14.260	498.70	870.29	1330.4	2791.8	4555.0	1104
20B4R + 1IHL2 × 2	14.263	498.76	870.38	1330.4	2791.8	4555.0	1464
20B4R + 1IHL3 × 3	14.263	497.15	864.86	1316.4	2727.1	4380.4	2379
20B4 + 1IHL3 × 3	14.227	496.85	864.37	1315.7	2726.2	4379.5	2379

[a]The number of elements is 2 × 40
[b]The number of elements is 3 × 50
[c]The number of elements is 2 × 40 × 2
[d]The number of elements is 3 × 50 × 3

5.2. Laminated beam

The second assessment aims to show the capability of the present model for a set of laminated beams with an anti-symmetric stacking sequence $[45^\circ/-45^\circ]_2$. The same geometrical size ($h/l, l = 1$ m) and boundary condition as those in the previous case are considered again (see Figure 5). Each lamina is of equal thickness and made of an orthotropic material with the following properties: $E_{11} = 76.0$ GPa, $E_{22} = E_{33} = 5.5$ GPa, $\nu_{12} = \nu_{13} = \nu_{23}$=0.34, $G_{12} = G_{13} = 2.3$ GPa, $G_{23} = 1.5$ GPa, $\alpha_1 = -4 \times 10^{-6}/^\circ$C, $\alpha_2 = \alpha_3 = 79 \times 10^{-6}/^\circ$C.

Table 2 provides a full comparative analysis between total and updated Lagrangian forms of 1 D CUF models, accompanied by a series of ABAQUS results used for reference purposes. When the kinematic order over the thickness of each layer is larger than or equal to 2, the computational cost of the proposed LW models increases dramatically, far exceeding that of the refined S8R element. Nonetheless, even for a very thin beam with h/l equal to 0.01, the first-order plate model obtained using the ESL approach, namely S8R, produces poor results. This inaccuracy is primarily due to nonlinear deformation along the thickness caused by anti-symmetric laminates. The even IHLE model with the first-order expansion in each layer cannot lead to results with improved accuracy. Notably, 20B4 + 4IHL3 × 2 with ULF is capable of producing more precise critical temperatures than the ABAQUS 3 D model using a low-fidelity mesh, although the two models being virtually identical in terms of DOF. However, due to the advantage of the aspect ratio of the beam element and the higher-order approximation of the deflection variation through the thickness, 4IHL4 × 3 with ULF can save more computational effort in terms of DOF without sacrificing the numerical accuracy of the solution compared to the ABAQUS 3 D reference model with a dense mesh. Additionally, the difference between IHLE-TLF and -ULF becomes evident from $h/l = 0.08$, which is smaller than that of the metallic counterparts mentioned in the previous sub-section. As a result of such the distinction, a linearized buckling analysis becomes useless, necessitating the use of a geometrically nonlinear analysis. Another unexpected and intriguing phenomena can be found when full and reduced integration schemes are compared. The difference becomes more pronounced as h/l raises for ABAQUS 3 D models and h/l equals 0.20 for IHLE-TLF models, but is minor for all h/l in the table for IHLE-TLF models. Indeed, 3 D elements apply reduced integration across the entire volume, while refined 1 D elements employ it

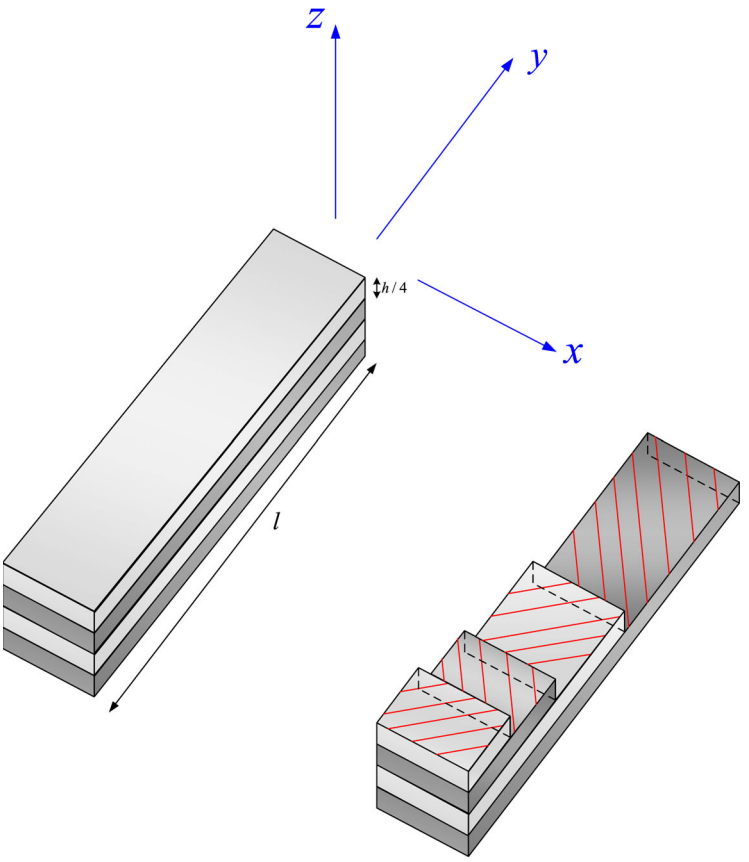

Figure 5. Geometric properties and lamination scheme of the four-layer laminated beam.

Table 2. Comparison of the critical temperatures of laminated beams for various thickness-to-length ratios.

	h / l						
Method	**0.01**	**0.06**	**0.08**	**0.10**	**0.15**	**0.20**	DOF
Abaqus-S8R[a]	66.518	2210.7	3695.7	5357.8	9593.5	13163	1950
Abaqus-S8R[b]	66.505	2211.7	3698.0	5362.1	9605.4	13169	3342
Abaqus-C3D20R[c]	25.517	894.09	1544.9	2323.8	4518.2	6396.8	6351
Abaqus-C3D20[c]	26.206	920.11	1591.5	2395.5	4657.3	6577.9	6351
Abaqus-C3D20R[d]	23.613	828.29	1432.8	2149.8	4187.8	5835.8	19935
Abaqus-C3D20[d]	23.848	836.88	1448.2	2175.8	4240.8	5979.8	19935
IHLE-TLF							
10B4 + 4IHL3 × 1	36.499	1216.5	2037.8	2962.4	5368.6	7451.8	1860
15B4 + 4IHL3 × 1	36.456	1217.4	2037.8	2962.0	5372.5	7504.4	2760
20B4 + 4IHL3 × 2	26.028	881.70	1488.7	2183.2	4041.1	5708.3	5856
20B4R + 4IHL4 × 3	23.410	802.48	1357.8	1994.1	3700.6	5219.0	8967
20B4 + 4IHL4 × 3	23.727	804.68	1359.4	1995.1	3704.4	5259.6	8967
IHLE-ULF							
10B4 + 4IHL3 × 1	36.550	1273.8	2197.6	3285.5	6032.1	7752.5	1860
15B4 + 4IHL3 × 1	36.507	1274.9	2197.8	3284.8	6030.9	7752.2	2760
20B4 + 4IHL3 × 2	26.056	914.66	1583.1	2384.6	4641.6	6562.1	5856
20B4R + 4IHL4 × 3	23.440	829.46	1435.6	2161.8	4217.0	5916.2	8967
20B4 + 4IHL4 × 3	23.750	831.83	1437.6	2163.4	4217.4	5916.6	8967

[a]The number of elements is 2 × 40
[b]The number of elements is 3 × 50
[c]The number of elements is 2 × 40 × 4
[d]The number of elements is 3 × 50 × 8

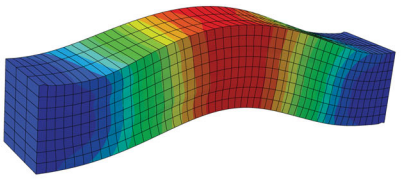

(a) ABAQUS solution with the full integration scheme

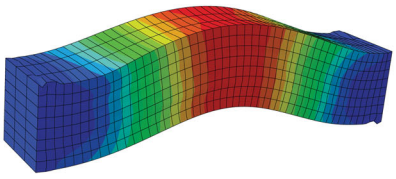

(b) ABAQUS solution with the reduced integration scheme

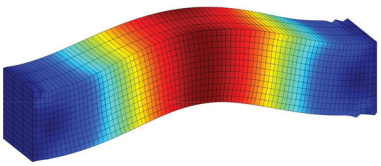

(c) IHLE-TLF solution with the full integration scheme

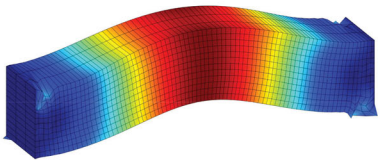

(d) IHLE-TLF solution with the reduced integration scheme

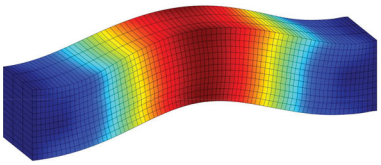

(e) IHLE-ULF solution with the full integration scheme

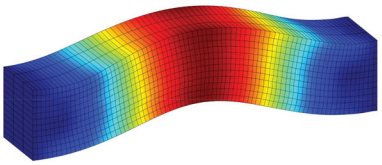

(f) IHLE-ULF solution with the reduced integration scheme

Figure 6. Comparison of the buckling modes computed by various CUF-IHLE models against ABAQUS solutions.

exclusively along the longitudinal direction. This means that reducing the number of integration points does not always result in a large increase in accuracy as in the preceding example, but can occasionally result in solution oscillation. The prominent difference in values with $h/l = 0.2$ can be further reflected in the buckling shapes in the 3 D space as shown in Figure 6. The plot clearly shows that irregular deformation occurs in varying degrees around both ends, among with IHLE-TLF being the most conspicuous regardless of the integration technique, followed by the ABAQUS model with a reduced integration strategy and finally the remaining models with flawless shapes.

5.3. Laminated plate

The purpose of this section is to compare the effects of different types of analyses, namely one-step and two-step analyses on the buckling values with respect to laminated plates oriented at $[\pm\theta]_s$. Each layer of the square cross-section is regarded to be equal in $h/l, l = 1$ m. The material property is identical to that in the previous one. The investigation regards three sets of boundary conditions, namely four edges clamped (CCCC), four edges simply supported (SSSS), and two opposite edges clamped and other sides simply supported (CSCS). Figure 7 denotes three sets of conditions mentioned above with the detailed mathematical formulation.

Figure 8 compares the critical temperatures of laminated plates given by various models with $\theta = 45^{\circ}$. For IHLE, $10B4 + 4IHL10 \times 2$ is adopted, and the number of elements in ABAQUS-3D is $30 \times 30 \times 4$, ensuring convergent results. The accuracy of the proposed model is demonstrated once again by the minuscule difference between ULF (Two-step analysis) and ABAQUS-3D

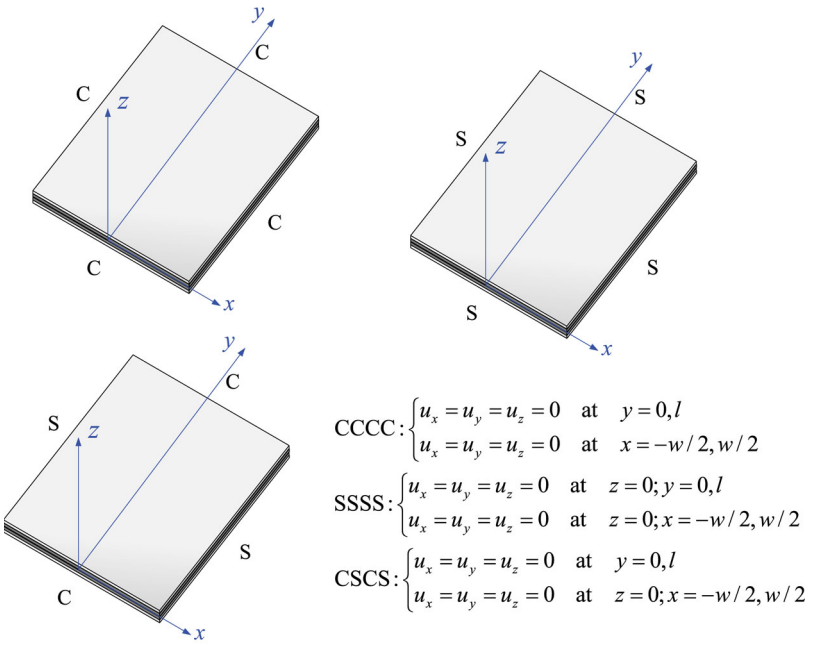

Figure 7. Three kinds of boundary conditions for square laminated plates.

models. Additionally, when h/l is less than or equal to 0.01 the computed values are not completely sensitive to the models. In other words, the cheapest computational approach, i.e., TLF (One-step analysis) is the best candidate for analyzing thermal buckling in thin structures. However, with an increase in h/l, particularly in the SSSS boundary condition, an apparent distinction can be detected.

Tables 3–5 gives a detailed comparison of IHLE-TLF and -ULF for the laminated plate with a set of ply angles, emphasizing the distinction between one-step and two-step analyses.

In general, the simple-supported condition provides lower bounds on critical temperatures by selectively relaxing boundary constraints, whereas the fully clamped condition presents upper bounds. IHLE-TLF predicts lower values than IHLE-ULF. Specifically, when h/l approaches 0.1, the deformed and original configurations become significantly identifiable, resulting in the greatest divergence between the values produced by the same CUF model with different buckling formulas. Additionally, the closer θ is to 45°, the more TLF deviates from ULF in terms of the critical temperature. This is because θ of 45° contributes significantly to structural heterogeneity throughout the thickness, demonstrating the nonlinear effect of cross-section deformation. As for the analysis step, one-step analysis within the framework of IHLE-TLF produces values that are closer to those obtained by the two-step analysis implemented in the IHLE-ULF framwork when h/l equals 0.01 and the boundary condition is CCCC, with a maximum difference of approximately 3.1% appearing at $\theta = 45^\circ$. This finding proves in turn the correctness of prior works [45,46], where the analysis procedure consisted solely of the solution of the eigenvalue problem given by Eq. (27). Therefore, when the influence of the pre-buckled deformation induced by the thermal force (see Eq. (31)) and S_{zz} can be safely ignored, TLF with one-step analysis can achieve optimal numerical efficiency while producing acceptable results. In comparison to ULF (two-step analysis), TLF (one-step analysis) performs poorly with $h/l = 0.1$, resulting in values with a minimum difference of 26.1% occurring at $\theta = 75^\circ$ under CSCS boundary condition. In fact, one-step analysis assumes a negligible out-of-plane normal stress (S_{zz}), leading to an in-plane problem in the pre-buckling stage. Obviously, both shear and normal deformation play a non-negligible role

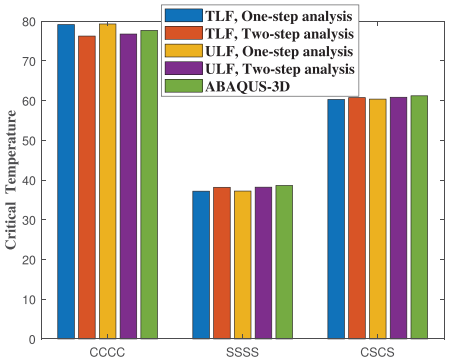

(a) $h/l = 0.01$

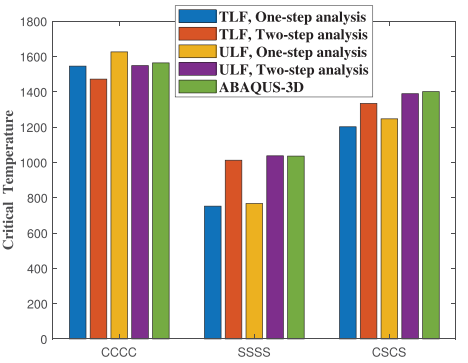

(b) $h/l = 0.05$

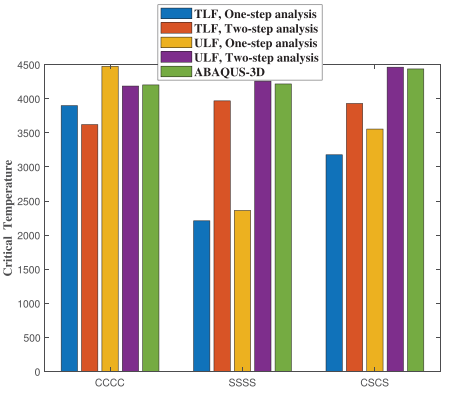

(c) $h/l = 0.1$

Figure 8. Graphical representation of the critical temperatures of laminated plates computed by different models.

Table 3. Buckling values of CCCC laminated plates corresponding to different types of analyses.

h / l	θ	IHLE-TLF		IHLE-ULF	
		One-step analysis	Two-step analysis	One-step analysis	Two-step analysis
0.01	0°	25.812	24.504	25.876	24.561
	15°	32.325	30.656	32.418	30.733
	30°	55.441	55.370	55.572	55.500
	45°	79.156	76.270	79.313	76.778
	60°	55.466	54.493	55.598	54.621
	75°	32.358	32.042	32.444	32.127
0.05	0°	504.72	483.17	531.17	507.82
	15°	605.50	580.56	632.75	612.46
	30°	1000.9	992.66	1056.0	1048.7
	45°	1545.8	1472.2	1626.3	1548.7
	60°	1000.9	978.81	1056.0	1033.9
	75°	605.39	597.56	632.68	625.06
0.1	0°	1286.1	1244.5	1449.8	1440.6
	15°	1484.8	1442.3	1687.6	1683.4
	30°	2358.4	2300.7	2740.2	2691.3
	45°	3898.9	3620.9	4476.3	4186.6
	60°	2358.4	2280.0	2740.2	2668.2
	75°	1484.6	1455.5	1687.5	1663.6

Table 4. Buckling values of SSSS laminated plates corresponding to different types of analyses.

h/l	θ	IHLE-TLF		IHLE-ULF	
		One-step analysis	Two-step analysis	One-step analysis	Two-step analysis
0.01	0°	11.356	11.370	11.365	11.380
	15°	15.821	15.848	15.836	15.863
	30°	31.893	32.166	31.934	32.208
	45°	37.210	38.187	37.242	38.220
	60°	31.888	32.317	31.929	32.360
	75°	15.816	15.917	15.831	15.932
0.05	0°	257.29	280.44	262.19	285.80
	15°	338.76	370.25	346.08	378.39
	30°	631.66	723.67	650.31	746.51
	45°	752.50	1012.7	767.38	1037.5
	60°	631.87	738.63	650.53	762.23
	75°	338.84	377.65	346.17	386.00
0.1	0°	809.80	1034.7	862.33	1103.4
	15°	1001.3	1279.2	1073.2	1374.9
	30°	1706.9	2303.3	1870.0	2552.5
	45°	2210.7	3969.4	2362.7	4258.4
	60°	1708.5	2327.5	1872.1	2603.0
	75°	1002.2	1302.5	1074.3	1404.4

Table 5. Buckling values of CSCS laminated plates corresponding to different types of analyses.

h/l	θ	IHLE-TLF		IHLE-ULF	
		One-step analysis	Two-step analysis	One-step analysis	Two-step analysis
0.01	0°	21.770	21.884	21.806	21.920
	15°	27.681	27.817	27.732	27.868
	30°	48.739	48.931	48.812	49.006
	45°	60.309	60.773	60.395	60.861
	60°	37.505	36.860	37.560	36.913
	75°	20.147	19.905	20.182	19.939
0.05	0°	425.88	477.06	441.02	494.12
	15°	518.00	580.44	538.58	604.11
	30°	874.28	1023.2	904.49	1063.7
	45°	1202.0	1334.4	1247.0	1389.3
	60°	773.18	739.34	800.83	764.47
	75°	430.60	413.61	447.55	429.62
0.1	0°	1110.6	1461.1	1239.3	1645.0
	15°	1302.2	1681.5	1466.6	1913.2
	30°	2076.5	2786.2	2288.1	3193.8
	45°	3178.6	3930.9	3556.1	4463.2
	60°	2096.6	2003.9	2359.3	2247.8
	75°	1231.7	1167.5	1388.9	1313.4

as structural h/l and inhomogeneity increase. In other words, the efficacy of one-step analysis in resolving the thermal buckling problem is contingent upon the boundary condition, geometrical size, and material property.

Additional innovative outcomes may be derived from the individual table. As seen in Table 3, one-step analysis always predicts higher values than two-step analysis with the same formulation adopted, which makes the structure in an unsecure area. When h/l is smaller than 0.05, these overestimated values correspond well with those obtained using two-step analysis (IHLE-ULF), indicating the possibility of using one-step analysis (IHLE-TLF) in this context. Another computationally efficient approach, one-step analysis (IHLE-ULF), demonstrates comparable capacity under such conditions and may be generalized to the situation of $h/l = 0.1$ excluding the ply angle at 45°. However, the conclusions reached above are not generally applicable. When it comes to Table 4, the results reach higher values with two-step analysis than with one-step one. Besides, substantial discrepancies occur between one-step (IHLE-TLF) and two-step (IHLE-ULF) analyses

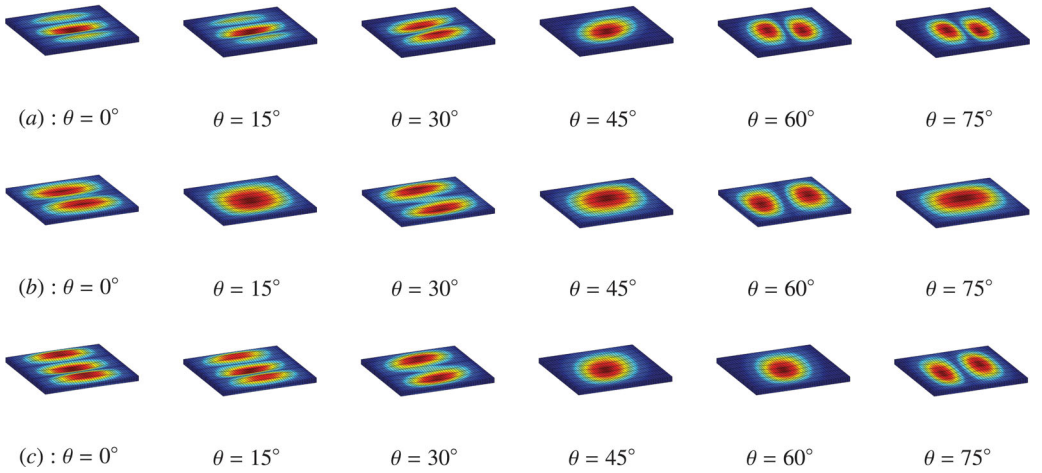

Figure 9. Buckling mode shapes of laminated plates subject to: (*a*) CCCC; (*b*) SSSS; (*c*) CSCS boundary conditions.

when h/l equals 0.05 and θ is inside in the interval $[30^{\circ}, 60^{\circ}]$. On the other hand, two-step analysis (IHLE-TLF) predicts somewhat smaller values with acceptable accuracy as an alternative to two-step analysis (IHLE-ULF). The inconsistency between one-step and two-step analyses (IHLE-TLF) reveals that decreased stiffness at boundaries may contribute to the amplification of the pre-buckled deformation. After evaluating the influence of boundary conditions denoted by single S and C, it will proceed to the one mixed with S and C. The results are summarized in Table 5. The discrepancy between one-step analysis (IHLE-TLF) and two-step (IHLE-ULF) analysis can be explained by the variation of θ. Smaller values are seen in one-step analysis until θ reaches 45°, from which point this relationship becomes inverse. And, once again, one-step analysis (IHLE-TLF) may be a possibility for the case of $h/l = 0.05$ due to conservative estimates for $\theta \leq 45^{\circ}$ and a maximum difference of almost 1.1% in the range $[60^{\circ}, 75^{\circ}]$.

Figure 9 illustrates 3 D buckling mode shapes of laminated plates with $h/l = 0.05$ under the boundary conditions discussed before. As can be seen in the figure, the mode shapes are dominated by a variable number of crests and troughs. At $\theta = 0^{\circ}, 15^{\circ}$, a triple undulation in the width direction occurs for the CCCC condition, with crests and troughs of variable magnitudes. $\theta = 30^{\circ}, 60^{\circ}, 75^{\circ}$ correspond to a double undulation with the same-valued crest and trough. At $\theta = 45^{\circ}$, a single-wave bending mode exists, which persists under all subsequent conditions. The SSSS condition softens the boundary restriction, resulting in a decrease in buckling values as well as the number of crests and troughs. Except for $\theta = 60^{\circ}$, the CSCS condition exhibits virtually identical modes to the CCCC condition.

6. Conclusions

The thermal buckling analysis of beam and plate structures is contrasted using linear incremental techniques based on total and updated Lagrangian formulations (TLF and ULF). Furthermore, 3 D stability equations can be obtained using the Carrera Unified Formulation-improved hierarchical Legendre expansion (CUF-IHLE) as a structural basis and 1 D Finite Element Method (FEM) as a numerical method. Due to the intrinsic advantage of CUF-based FEM models, the governing equations in terms of TLF and ULF are concisely defined using fundamental nuclei. A rigorous numerical evaluation of the critical temperature of metallic and composite beams and plates has been conducted in order to illustrate the increased accuracy and efficacy of the proposed model. The following is a summary of several major findings from this investigation:

1. S8R, as a typical 2D element in ABAQUS, is capable of discriminating the critical temperature of thin structures with strong homogeneity, e.g., isotropic materials or symmetric laminates. 3D elements are qualified to perform all perfect buckling analyses with regard to accuracy, particularly in heterogeneous structures with anti-symmetric lamination schemes, where S8R fails. This is not the case with CUF-IHLE, which, due to its variable-kinematic features, can provide an advantageous tradeoff between accuracy and computational cost.
2. In contrast to improved accuracy in static and free vibration analyses, the reduced integration scheme in 3D elements for linearized buckling analysis cannot achieve the same performance as the thickness-to-length ratio increases, but rather results in irregular deformation at the boundary. Nevertheless, in the proposed higher-order 1D formulation, such an integration that operates exclusively on 1D elements has a negligible effect on the magnitude of the value.
3. For panels with a high degree of heterogeneity and a large thickness-to-length ratio, the nonlinear influence of displacement fields across the thickness becomes apparent, explaining the inconsistencies between TLF and ULF results. This discrepancy, meanwhile, demonstrates that the current and initial configurations are distinct, necessitating the application of post-buckling analysis that is computationally expensive.
4. If a homogeneous temperature change is assumed, both in-plane and out-of-plane strains at the pre-buckling stage can be omitted for thin symmetric laminates or thin isotropic panels with some particular boundary conditions, e.g., four edges clamped or simply supported. Thus, the ensuing uniform distribution of pre-buckling stresses allows for pure eigenvalue analysis, i.e., one-step analysis. Otherwise, knowledge of the pre-buckling stress is required prior to conducting the subsequent eigenvalue analysis, resulting in the so-called two-step analysis.

The thermal buckling of multilayer composite laminates as predicted by TLF and ULF-based CUF-IHLE models is compared in this study. Although this article considers just uniform a temperature change, more advanced composite materials, such as functionally graded composites, typically suffer temperature changes that vary across the thickness. The proposed model will be extended to the uncertainty analysis on the thermal buckling behavior of these types of structures in the future.

Funding

Yang Yan acknowledges funding from the National Natural Science Foundation of China (Grant No. 12002012). Alfonso Pagani acknowledges funding from the European Research Council (ERC) under the European Union's Horizon 2020 research and innovation programme (Grant agreement No. 850437).

ORCID

Alfonso Pagani http://orcid.org/0000-0001-9074-2558

References

[1] E. Carrera, F. A. Fazzolari and M. Cinefra, *Thermal Stress Analysis of Composite Beams, Plates and Shells: Computational Modelling and Applications*. Cambridge: Academic Press, 2016,
[2] S. Timoshenko, *Theory of Elastic Stability 2e*. New York: Tata McGraw-Hill Education, 1970,
[3] I. Elishakoff and O. Rollot, "New closed-form solutions for buckling of a variable stiffness column by mathematica," *J. Sound Vibration.*, vol. 224, no. 1, pp. 172–182, 1999. DOI: 10.1006/jsvi.1998.2143.

[4] I. Elishakoff, "Inverse buckling problem for inhomogeneous columns," *Int. J. Solids Struct.*, vol. 38, no. 3, pp. 457–464, 2001. DOI: 10.1016/S0020-7683(00)00049-4.
[5] G. Catellani and I. Elishakoff, "Apparently first closed-form solutions of semi-inverse buckling problems involving distributed and concentrated loads," *Thin-Walled Struct.*, vol. 42, no. 12, pp. 1719–1733, 2004. DOI: 10.1016/j.tws.2004.05.007.
[6] S. R. Li and R. C. Batra, "Thermal buckling and postbuckling of euler-bernoulli beams supported on nonlinear elastic foundations," *AIAA J.*, vol. 45, no. 3, pp. 712–720, 2007. DOI: 10.2514/1.24720.
[7] B. V. Sankar and J. T. Tzeng, "Thermal stresses in functionally graded beams," *AIAA J.*, vol. 40, no. 6, pp. 1228–1232, 2002. DOI: 10.2514/2.1775.
[8] T. C. Mathew, G. Singh and G. V. Rao, "Thermal buckling of cross-ply composite laminates," *Comput. Struct.*, vol. 42, no. 2, pp. 281–287, 1992. DOI: 10.1016/0045-7949(92)90212-I.
[9] R. C. Kar and T. Sujata, "Parametric instability of timoshenko beam with thermal gradient resting on a variable Pasternak foundation," *Comput. Struct.*, vol. 36, no. 4, pp. 659–665, 1990. DOI: 10.1016/0045-7949(90)90081-C.
[10] S. Wang, "A unified timoshenko beam b-spline rayleigh–ritz method for vibration and buckling analysis of thick and thin beams and plates," *Int. J. Numer. Meth. Engng*, vol. 40, no. 3, pp. 473–491, 1997. DOI: 10.1002/(SICI)1097-0207(19970215)40:3<473::AID-NME75>3.0.CO;2-U.
[11] T. Morimoto, Y. Tanigawa and R. Kawamura, "Thermal buckling analysis of inhomogeneous rectangular plate due to uniform heat supply," *J. Thermal Stresses*, vol. 26, no. 11-12, pp. 1151–1170, 2003. DOI: 10.1080/714050877.
[12] M. R. Prabhu and R. Dhanaraj, "Thermal buckling of laminated composite plates," *Comput. Struct.*, vol. 53, no. 5, pp. 1193–1204, 1994. DOI: 10.1016/0045-7949(94)90166-X.
[13] X. Li, K. Yu, J. Han, H. Song and R. Zhao, "Buckling and vibro-acoustic response of the clamped composite laminated plate in thermal environment," *Int. J. Mech. Sci.*, vol. 119, pp. 370–382, 2016. DOI: 10.1016/j.ijmecsci.2016.10.021.
[14] M. Mohammadabadi, A. R. Daneshmehr and M. Homayounfard, "Size-dependent thermal buckling analysis of micro composite laminated beams using modified couple stress theory," *Int. J. Engng. Sci.*, vol. 92, pp. 47–62, 2015. DOI: 10.1016/j.ijengsci.2015.03.005.
[15] F. Ebrahimi and E. Salari, "Thermal buckling and free vibration analysis of size dependent Timoshenko FG nanobeams in thermal environments," *Composite Struct.*, vol. 128, pp. 363–380, 2015. DOI: 10.1016/j.compstruct.2015.03.023.
[16] E. Taati, "On buckling and post-buckling behavior of functionally graded micro-beams in thermal environment," *Int. J. Engng. Sci.*, vol. 128, pp. 63–78, 2018. DOI: 10.1016/j.ijengsci.2018.03.010.
[17] Y. Z. Wang, H. T. Cui, F. M. Li and K. Kishimoto, "Thermal buckling of a nanoplate with small-scale effects," *Acta Mech.*, vol. 224, no. 6, pp. 1299–1307, 2013. DOI: 10.1007/s00707-013-0857-7.
[18] M. H. Shojaeefard, H. S. Googarchin, M. Ghadiri and M. Mahinzare, "Micro temperature-dependent fg porous plate: Free vibration and thermal buckling analysis using modified couple stress theory with cpt and fsdt," *APPl. Math. Modelling*, vol. 50, pp. 633–655, 2017. DOI: 10.1016/j.apm.2017.06.022.
[19] B. Omidvar, "Shear coefficient in orthotropic thin-walled composite beams," *J. Compos. Constr.*, vol. 2, no. 1, pp. 46–56, 1998. DOI: 10.1061/(ASCE)1090-0268(1998)2:1(46).
[20] P. Madabhusi-Raman and J. F. Davalos, "Static shear correction factor for laminated rectangular beams," *Composites Part B Engng.*, vol. 27, no. 3-4, pp. 285–293, 1996. DOI: 10.1016/1359-8368(95)00014-3.
[21] M. Lezgy-Nazargah, "Fully coupled thermo-mechanical analysis of bi-directional fgm beams using nurbs isogeometric finite element approach," *Aerospace Sci. Technol.*, vol. 45, pp. 154–164, 2015. DOI: 10.1016/j.ast.2015.05.006.
[22] N. Shafiei and G. L. She, "On vibration of functionally graded nano-tubes in the thermal environment," *Int. J. Engng. Sci.*, vol. 133, pp. 84–98, 2018. DOI: 10.1016/j.ijengsci.2018.08.004.
[23] M. Aydogdu, "Thermal buckling analysis of cross-ply laminated composite beams with general boundary conditions," *Composites Sci. Technol.*, vol. 67, no. 6, pp. 1096–1104, 2007. DOI: 10.1016/j.compscitech.2006.05.021.
[24] J. N. Reddy, "A simple higher-order theory for laminated composite plates," *J. Appl. Mech.*, vol. 51, no. 4, pp. 745–752, 1984. DOI: 10.1115/1.3167719.
[25] K. P. Soldatos, "A transverse shear deformation theory for homogeneous monoclinic plates," *Acta Mechanica*, vol. 94, no. 3-4, pp. 195–220, 1992. DOI: 10.1007/BF01176650.
[26] M. Karama, K. S. Afaq and S. Mistou, "Mechanical behaviour of laminated composite beam by the new multi-layered laminated composite structures model with transverse shear stress continuity," *Int. J. Solids Struct.*, vol. 40, no. 6, pp. 1525–1546, 2003. DOI: 10.1016/S0020-7683(02)00647-9.
[27] V. N. Van Do and C. H. Lee, "Quasi-3d isogeometric buckling analysis method for advanced composite plates in thermal environments," *Aerospace Sci. Technol.*, vol. 92, pp. 34–54, 2019. DOI: 10.1016/j.ast.2019.05.056.

[28] M. Cetkovic, "Thermal buckling of laminated composite plates using layerwise displacement model," *Composite Struct.*, vol. 142, pp. 238–253, 2016. DOI: 10.1016/j.compstruct.2016.01.082.
[29] M. Shariyat, "Thermal buckling analysis of rectangular composite plates with temperature-dependent properties based on a layerwise theory," *Thin-Walled Struct.*, vol. 45, no. 4, pp. 439–452, 2007. DOI: 10.1016/j.tws.2007.03.004.
[30] W. T. Koiter, "A consistent first approximations in the general theory of thin elastic shells," in *Proceedings of First Symposium on the Theory of Thin Elastic Shells*, pp. 12–23. North-Holland, Amsterdam, 1959,
[31] E. Carrera, "Theories and finite elements for multilayered plates and shells: A unified compact formulation with numerical assessment and benchmarking," *ARCO*, vol. 10, no. 3, pp. 215–296, 2003. DOI: 10.1007/BF02736224.
[32] E. Carrera, "Theories and finite elements for multilayered, anisotropic, composite plates and shells," *ARCO*, vol. 9, no. 2, pp. 87–140, 2002. DOI: 10.1007/BF02736649.
[33] E. Carrera, G. Giunta and M. Petrolo, *Beam Structures: Classical and Advanced Theories*. Hoboken: John Wiley & Sons, 2011,
[34] P. Nali, E. Carrera and S. Lecca, "Assessments of refined theories for buckling analysis of laminated plates," *Composite Struct.*, vol. 93, no. 2, pp. 456–464, 2011. DOI: 10.1016/j.compstruct.2010.08.035.
[35] F. A. Fazzolari and E. Carrera, "Thermo-mechanical buckling analysis of anisotropic multilayered composite and sandwich plates by using refined variable-kinematics theories," *J. Thermal Stresses*, vol. 36, no. 4, pp. 321–350, 2013. DOI: 10.1080/01495739.2013.770642.
[36] R. Vescovini, M. D'Ottavio, L. Dozio and O. Polit, "Buckling and wrinkling of anisotropic sandwich plates," *Int. J. Engng. Sci.*, vol. 130, pp. 136–156, 2018. DOI: 10.1016/j.ijengsci.2018.05.010.
[37] S. M. Ibrahim, E. Carrera, M. Petrolo and E. Zappino, "Buckling of composite thin walled beams by refined theory," *Composite Struct.*, vol. 94, no. 2, pp. 563–570, 2012. DOI: 10.1016/j.compstruct.2011.08.020.
[38] E. Carrera, A. Pagani and J. R. Banerjee, "Linearized buckling analysis of isotropic and composite beam-columns by carrera unified formulation and dynamic stiffness method," *Mech. Adv. Mater. Struct.*, vol. 23, no. 9, pp. 1092–1103, 2016. DOI: 10.1080/15376494.2015.1121524.
[39] A. Pagani and A. R. Sanchez-Majano, "Influence of fiber misalignments on buckling performance of variable stiffness composites using layerwise models and random fields," *Mech. Adv. Mater. Struct.*, In press.
[40] A. R. Sanchez-Majano, A. Pagani, M. Petrolo and C. Zhang, "Buckling sensitivity of tow-steered plates subjected to multiscale defects by high-order finite elements and polynomial chaos expansion," *Materials*, vol. 14, no. 11, pp. 2706, 2021. DOI: 10.3390/ma14112706.
[41] Y. Yan, B. Liu, Y. Xing, E. Carrera and A. Pagani, "Free vibration analysis of variable stiffness composite laminated beams and plates by novel hierarchical differential quadrature finite elements," *Composite Struct.*, vol. 274, pp. 114364, 2021. DOI: 10.1016/j.compstruct.2021.114364.
[42] Y. Yan, E. Carrera and A. Pagani, "Free vibration analysis of curved metallic and composite beam structures using a novel variable-kinematic dq method," *Mech. Adv. Mater. Struct.*, pp. 1–27, 2021. DOI: 10.1080/15376494.2021.1909784.
[43] E. Carrera, "C_Z^0 requirements-models for the two dimensional analysis of multilayered structures," *Composite Struct.*, vol. 37, no. 3-4, pp. 373–383, 1997. DOI: 10.1016/S0263-8223(98)80005-6.
[44] A. Pagani, A. G. De Miguel, M. Petrolo and E. Carrera, "Analysis of laminated beams via unified formulation and legendre polynomial expansions," *Composite Struct.*, vol. 156, pp. 78–92, 2016. DOI: 10.1016/j.compstruct.2016.01.095.
[45] F. M. Li and Z. G. Song, "Flutter and thermal buckling control for composite laminated panels in supersonic flow," *J. Sound Vibration*, vol. 332, no. 22, pp. 5678–5695, 2013. DOI: 10.1016/j.jsv.2013.05.032.
[46] K. Zhou, J. Su and H. Hua, "Aero-thermo-elastic flutter analysis of supersonic moderately thick orthotropic plates with general boundary conditions," *Int. J. Mech. Sci.*, vol. 141, pp. 46–57, 2018. DOI: 10.1016/j.ijmecsci.2018.03.026.
[47] E. Carrera, "Transverse normal strain effect on thermal stress analysis of homogeneous and layered plates," *AIAA J.*, vol. 43, no. 10, pp. 2232–2242, 2005. DOI: 10.2514/1.11230.
[48] R. Vescovini, M. D'Ottavio, L. Dozio and O. Polit, "Thermal buckling response of laminated and sandwich plates using refined 2-d models," *Composite Struct.*, vol. 176, pp. 313–328, 2017. DOI: 10.1016/j.compstruct.2017.05.021.
[49] N. H. Kim, *Introduction to Nonlinear Finite Element Analysis*. Berlin: Springer Science & Business Media, 2014,
[50] H. Noguchi and T. Hisada, "Integrated fem formulation for total/updated-lagrangian method in geometrically nonlinear problems," *JSME Int. J. Serious A, Mech. Mater. Engng*, vol. 38, no. 1, pp. 23–29, 1995. DOI: 10.1299/jsmea1993.38.1_23.
[51] A. Varello, "Advanced higher-order one-dimensional models for fluid-structure interaction analysis," Ph.D. dissertation, Politecnico di Torino, Turin, Italy, 2013.

[52] E. Carrera, M. Cinefra, M. Petrolo and E. Zappino, *Finite Element Analysis of Structures through Unified Formulation*. Hoboken: John Wiley & Sons, 2014,

[53] E. Carrera, A. G. De Miguel and A. Pagani, "Hierarchical theories of structures based on legendre polynomial expansions with finite element applications," *Int. J. Mech. Sci.*, vol. 120, pp. 286–300, 2017. DOI: 10.1016/j.ijmecsci.2016.10.009.

[54] J. N. Reddy, *Mechanics of Laminated Composite Plates and Shells: Theory and Analysis*. Boca Raton: CRC Press, 2004,